

therefore, decreasing wavelength. The two dispersion relations differ considerably at large wavelengths.

The fundamental, geometric definition of phase velocity is shown in Figure 6.31, where the dispersion relation for the gradually increasing shear wave velocity profile is shown. The phase velocity as a function of frequency and wavenumber equals the slope from the origin to the point on the dispersion relation corresponding to the particular frequency-wavenumber pair. For additional reference, the group velocity, which equals the instantaneous slope of the dispersion relation, is shown for reference. A profile with gradually decreasing shear wave velocity would bend downward rather than upward as the wavenumber decreased.

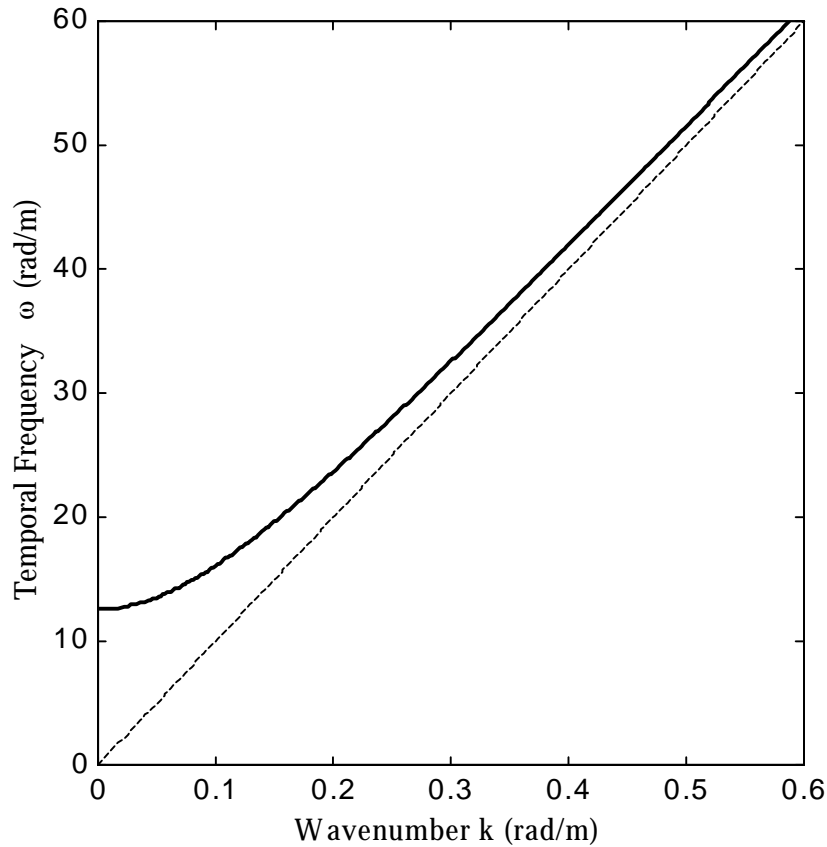


Figure 6.30 Dispersion Relation for a Heterogeneous Half-Space with Gradually Increasing Shear Wave Velocity  $V_S$  with Depth. The half-space has a minimum  $V_S = 108.76$  m/s at the surface, and the  $V_S$  gradually increases to infinity with increasing depth. The homogeneous half-space dispersion relation (dashed line) is shown for reference.

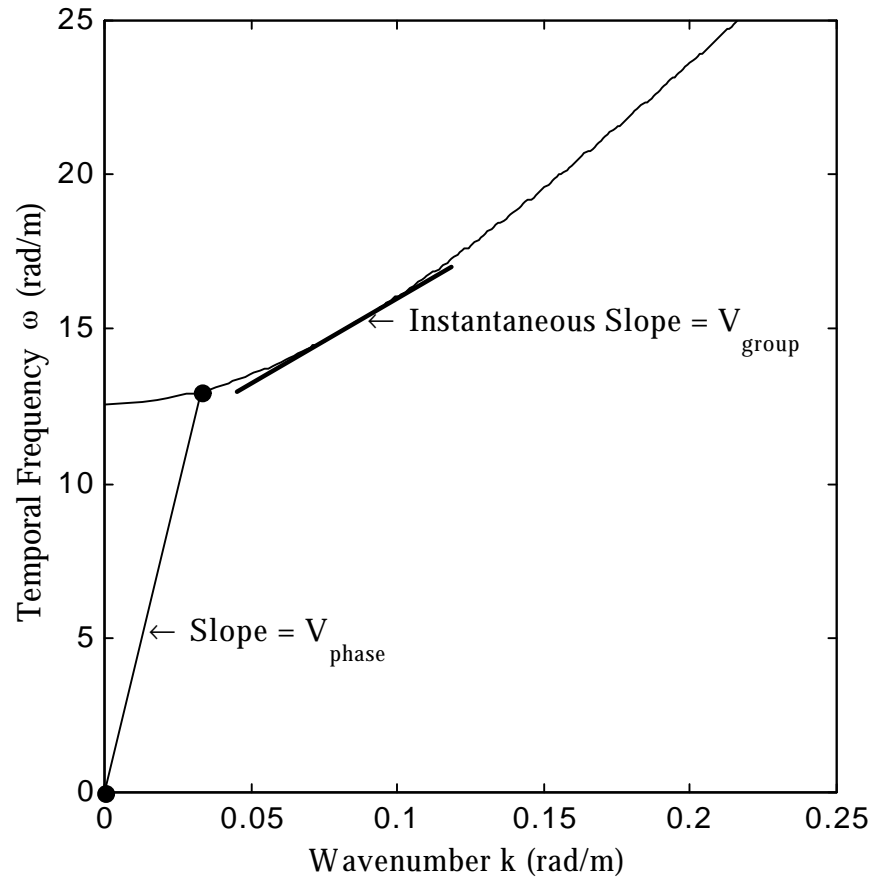


Figure 6.31 Group and Phase Velocity Definitions (After Johnson and Dudgeon, 1993)

### 6.10.3 Traditional Two-point SASW Dispersion Curve Estimators

The traditional dispersion curve estimates are obtained from averaging measurements of phase change for various spatial lags over a range of frequencies. The traditional two-point estimates for a homogeneous half-space with a Poisson's ratio  $\nu = 0.25$  and  $V_S = 108.7$  m/s will be analyzed in detail to determine the consequences of the modeling incompatibility on the phase velocity estimates.

Figure 6.32 shows the traditional two-point dispersion curve estimates for a homogeneous half-space. The graph simply represents the estimates of phase velocity due to modeling a cylindrically spreading wavefield with a plane wave model. The incorrect, lower phase velocity estimates at lower frequencies have previously been attributed to coupling of near-field surface and body waves (Sanchez-Salinero, 1987).

The model incompatibility completely explains the lower surface wave phase velocities at lower frequencies for a homogeneous half-space. Figure 6.33 shows the unwrapped phase for plane wave and cylindrical wave propagation for a wavenumber = 0.62 rad/m, corresponding to a frequency = 10 Hz in Figure 6.32. Although wavenumber is constant, the phase change versus distance is not linear for a cylindrical wave. Instead, the phase change is greater near the source, as seen in the right panel of Figure 6.33. Figure 6.34 shows the effect of the model incompatibility on the traditional cross power and transfer function two-point estimators. In the case of a homogeneous half-space, both methods overestimate the wavenumber, and the transfer function method estimates a larger wavenumber than the cross power spectrum method, as shown in the left panel of Figure 6.35. As the measurement distance from the source increases, both phase velocity estimation methods tend asymptotically to the correct estimate, as shown in the right panel of Figure 6.35.

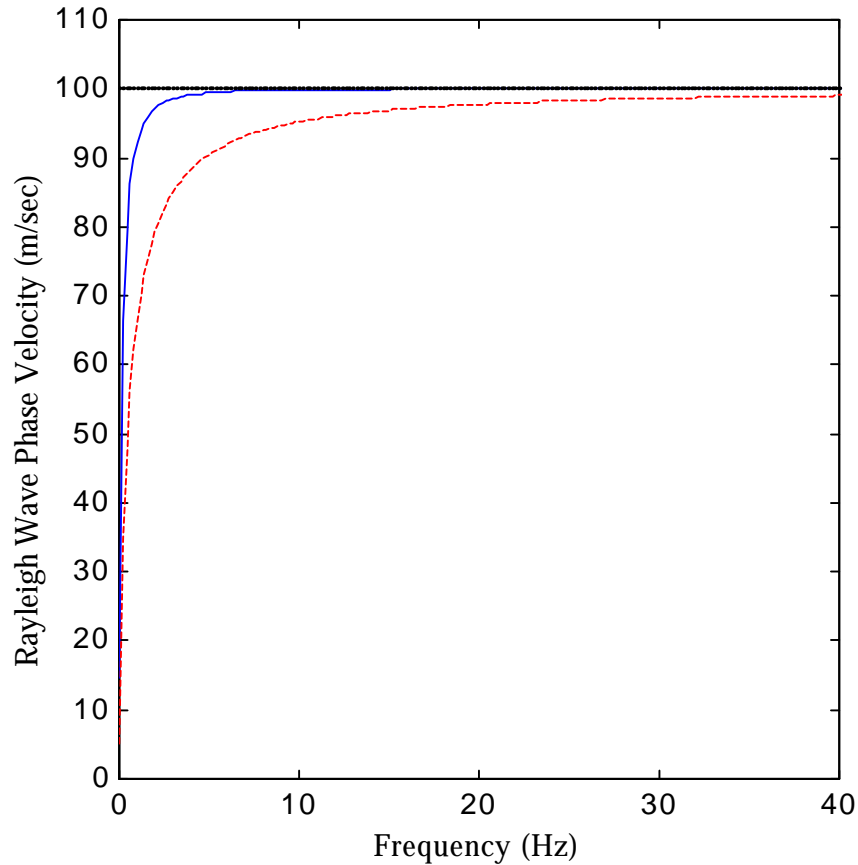


Figure 6.32 Traditional Transfer Function (dashed) and Cross Power (solid) Dispersion Curve Estimates for a Homogeneous Half-Space with  $V_R = 100$  m/s. The receivers are placed at  $d_1 = \lambda_{(10 \text{ Hz})} = 10$  m and  $d_2 = 20$  m for the cross power spectrum method, and the sensors for the transfer function method are placed at the source location and a distance of 15 m.

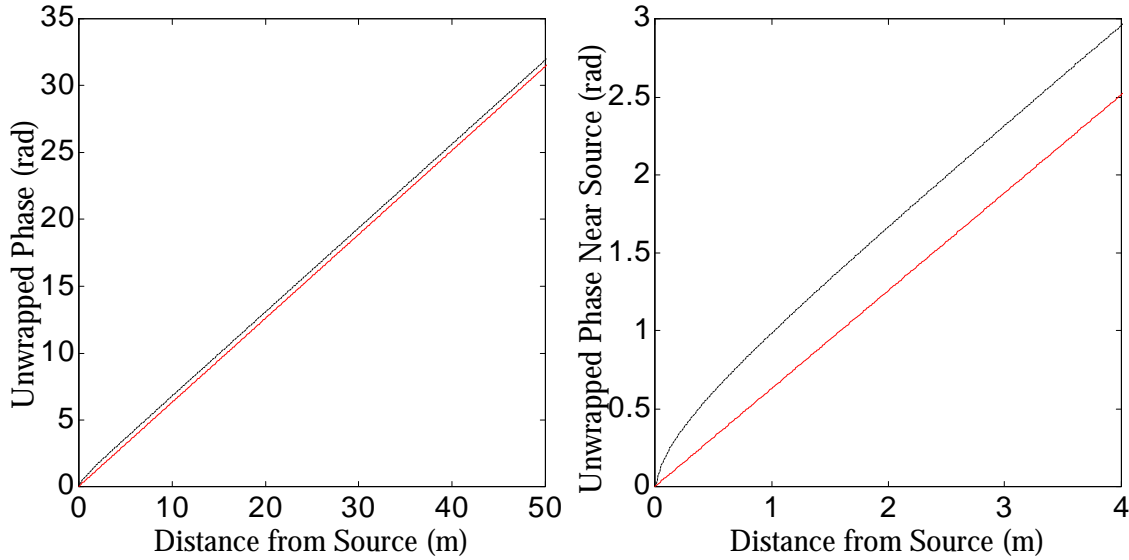


Figure 6.33 Unwrapped Phase for a Plane Wave (solid line) and Cylindrical Wave (dashed line) at 10 Hz for a Homogeneous Half-Space. The right panel shows a close-up of the left panel to emphasize the curved phase change for the cylindrical model near the source.

In a plot of phase velocity versus frequency in the homogeneous case, the phase velocity estimated from the transfer function method would always be lower than the cross power spectrum traditional estimator. Figure 6.36 shows the percent error (in dB's) of the two estimators for a surface wave wavelength = 10 m. The common bounds on the near-field recommendations in the geotechnical field are one-half wavelength in normally dispersive media and two wavelengths in inversely dispersive media. At one-half wavelength from the source, the error for the cross power spectrum method in a homogeneous half-space is about one percent (0 dB), while the transfer function method is still about 10 percent (20 dB). At two wavelengths from the source (20 m), the cross power method has less than 0.1 percent (-20 dB) error, but the transfer function method still has about a four percent error (10 dB). Therefore, the error traditionally associated with near-field and body wave interference effects is primarily caused by the model incompatibility of plane wave estimators in a cylindrical wavefield. Table 6.1 summarizes the model incompatibility effects on the traditional two-point phase velocity estimators.

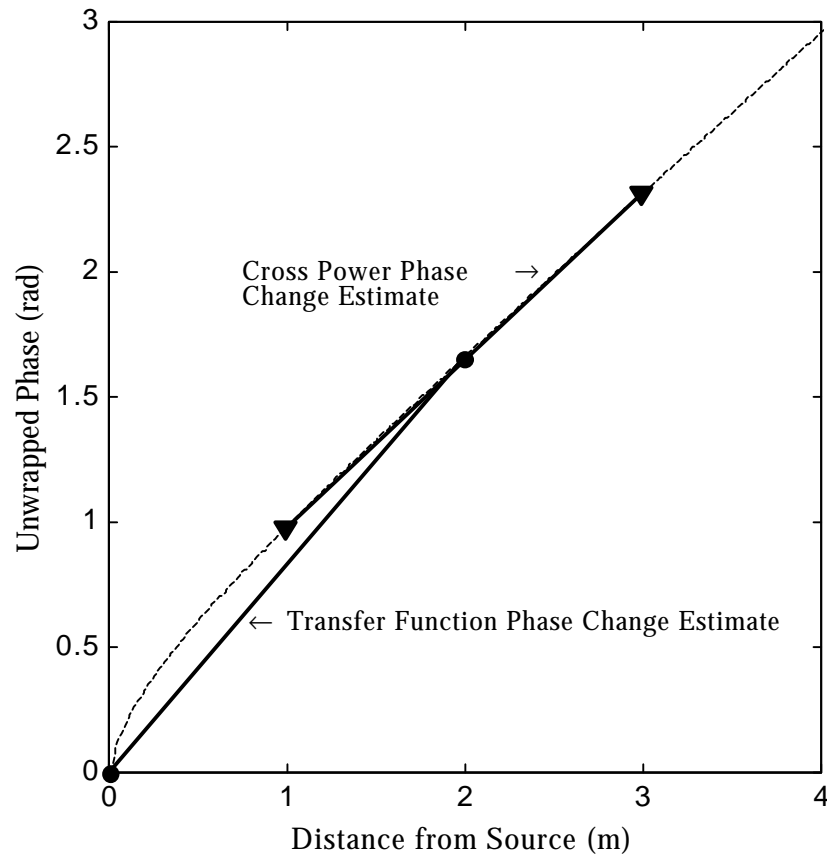


Figure 6.34 Traditional Cross Power and Transfer Function Phase Change Estimates for a Homogeneous Half-Space

Table 6.1 Model Incompatibility Effects on Traditional Phase Velocity Estimators for a Homogeneous, Elastic, Isotropic Half-Space

Traditional Estimator	$\frac{1}{2}$ Wavelength from Source	2 Wavelengths from Source
Cross Power	1 %	Less than 0.1 %
Transfer Function	10 %	4 %

Figure 6.37 shows the dispersion relation for the traditional estimators compared to the correct, homogenous, elastic, isotropic half-space case. The traditional estimators tend to the correct estimate at large frequencies and wavenumbers, but the estimate errors are considerably acute at lower frequencies and wavenumbers.

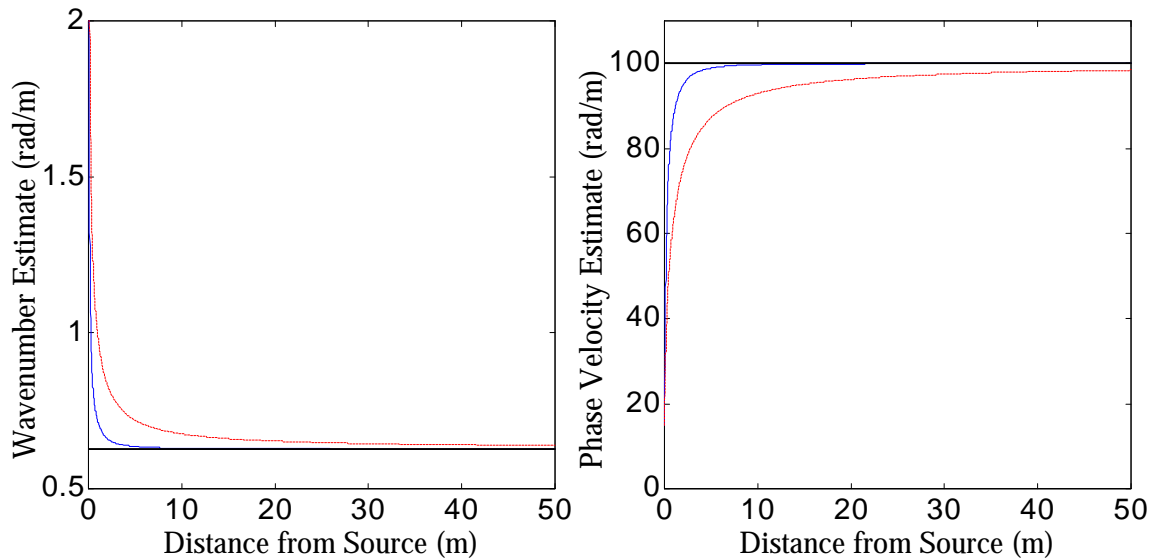


Figure 6.35 Traditional Two-Point Method Wavenumber (left panel) and Phase Velocity Estimates (right panel) as a Function of Measurement Distance from the Source. The cross power (solid line), transfer function (dashed line), and correct  $V_R = 100$  m/s are shown for frequency = 10 Hz ( $\lambda_{(10 \text{ Hz})} = 10$  m). Notice as the distance from the source increases, the phase velocity estimates asymptotically converge to the correct estimate. The transfer function method suffers larger estimation errors from the model incompatibility effects.

#### 6.10.4 Effects of Model Incompatibility

Although the effects may seem insignificant for engineering analysis, since in ideal conditions the error in estimated phase velocity is generally less than five percent, the consequences of the model incompatibility in geotechnical analysis of surface waves are far more insidious. Not only has the model incompatibility led to inappropriate conclusions regarding phase velocity estimation, but also regarding material attenuation. The present section discusses the consequences pertaining to phase velocity estimation, while Chapter 7 treats the effects on material attenuation.

First, the results from traditional Rayleigh phase velocities, even in the most ideal situation, are biased. Second, the inapplicability of the far-field, plane wave assumption has led to a whole field of conflicting and qualitative literature concerning the mitigation of near-field effects due to body waves. Third, the abilities of active surface wave methods for near surface geotechnical site investigation at lower frequencies have been unduly constrained, minimizing the potential usefulness of the method. Fourth, the large scatter of data and qualitative data inclusion decisions for phase velocity estimates due to the model incompatibility have decreased the acceptability of the method with practicing engineers. Each of the consequences mentioned will now be more fully discussed.

#### 6.10.4.1 Traditional Active Source Rayleigh Phase Velocity Estimators are Biased

Regardless of how far from the source measurements are made, the traditional two-point phase velocity estimators for a single mode of surface wave propagation are biased. As the far-field assumption becomes more acceptable with increasing distance from the source, the traditional phase velocity estimators asymptotically approach the correct value. Therefore, although the estimates are biased, they are asymptotically unbiased as distance from the source tends to infinity. In many engineering applications, biased, but asymptotically unbiased, estimates are used successfully. In fact, even the advanced plane wave power spectrum estimators discussed in Section 6.7 are biased for a cylindrically spreading wavefield. For geotechnical surface wave analysis, implementing the appropriate wavefield model leads to unbiased phase velocity estimates.

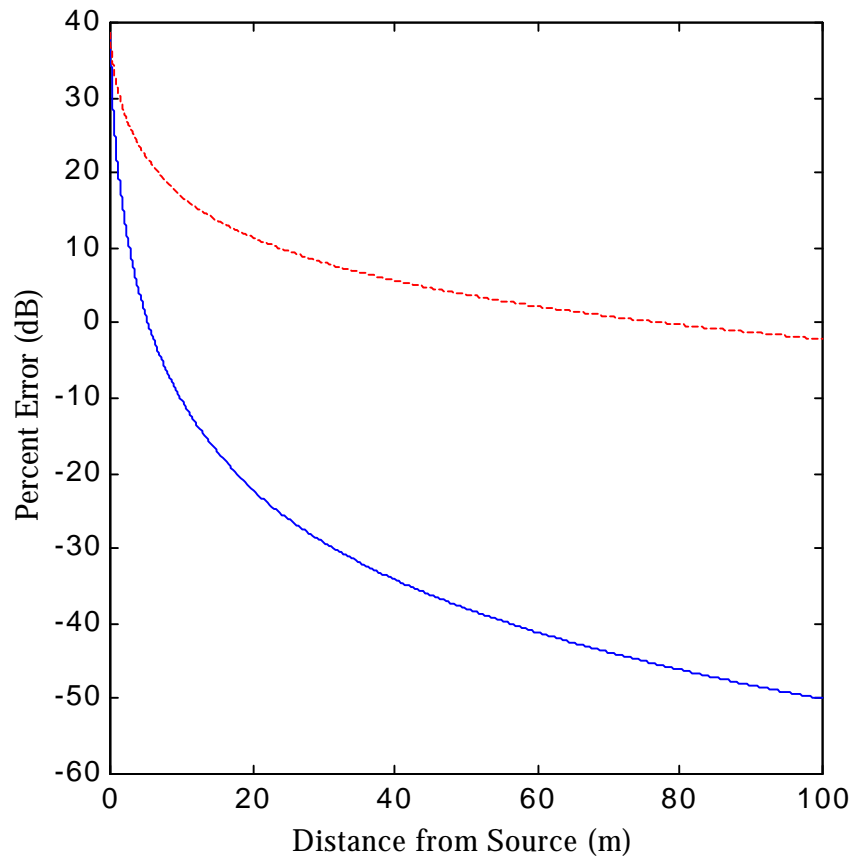


Figure 6.36 Percent Error (dB) for Traditional Transfer Function (dashed line) and Cross Power (solid line) Phase Velocity Estimators, for  $\lambda = 10$  m, as a Function of Measurement Distance from Source

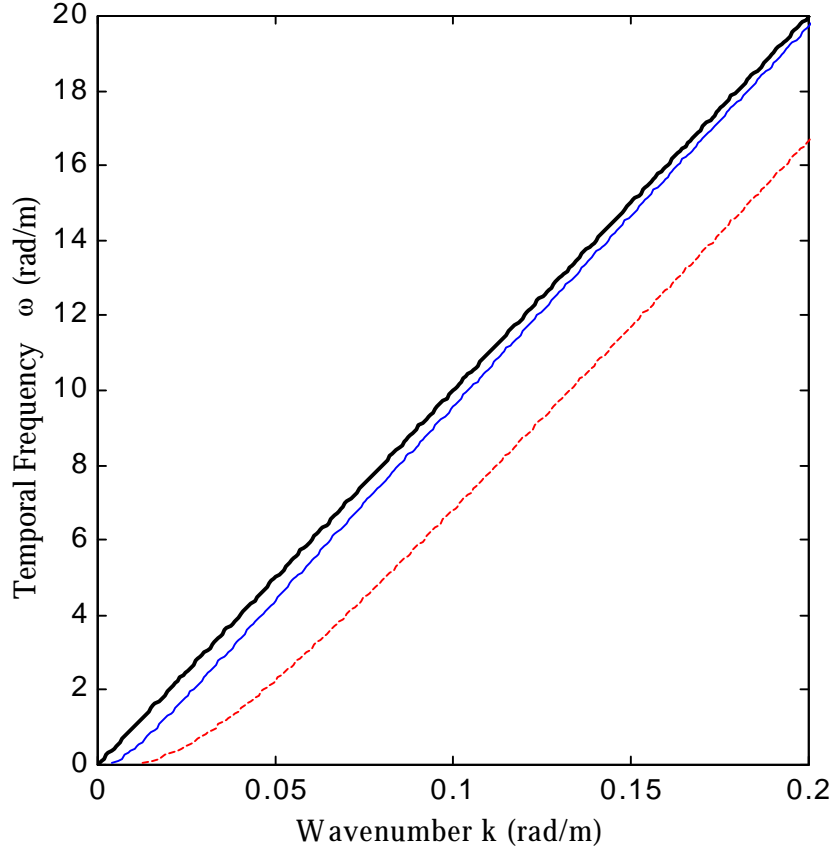


Figure 6.37 Dispersion Relation for the Traditional Transfer Function (dashed line) and Cross Power (light solid line) Estimators for a Homogeneous, Elastic, Isotropic Half-Space. The correct dispersion relation is shown in the dark solid line. Notice the much larger estimation error of the transfer function method and the persistence of the estimator bias as frequency and wavenumber increase.

The asymptotic property of the phase velocity estimators can easily be visualized, and the geometric visualization will help to understand some previous results found from numerical simulation of active source surface wave tests. Figure 6.38 shows a series of dispersion curves for an ideal, uniform half-space. Using dimensionless units, the  $V_S$  of the half-space equals 1.0, yielding a Rayleigh wave phase velocity of about 0.92. Phase velocities are estimated at distances from the source equal to 0.75, 1.5, and 3.0 units. Therefore, the sensor positions for the traditional cross power estimator are  $d_1 = 0.5$ , 1.0, and 2.0, respectively, and  $d_2 = 2d_1$ . In the case of the two-point transfer function method, sensors are located at the source and at  $d_1 = 0.75$ , 1.5, and 3.0. Notice that as the distance from the source becomes larger, both traditional estimation methods tend to the constant phase velocity of the homogeneous half-space. Also notice, as expected, the traditional

two-point cross power dispersion curve estimator converges much more rapidly than the transfer function estimator and yields smaller bias.

#### 6.10.4.2 Near-field Filtering Requirements are Qualitative and Conflicting

Table 6.2 reproduces a summary of the surface wave test near-field mitigation and spatial filtering criterion from Ganji, et al. (1998). Although referred to as “filtering” criteria in the geotechnical literature, the recommendations really are not filters in a signal processing sense. The recommendations are simply qualitative observations stemming from methods that appear to work well in experimental and numerical studies.

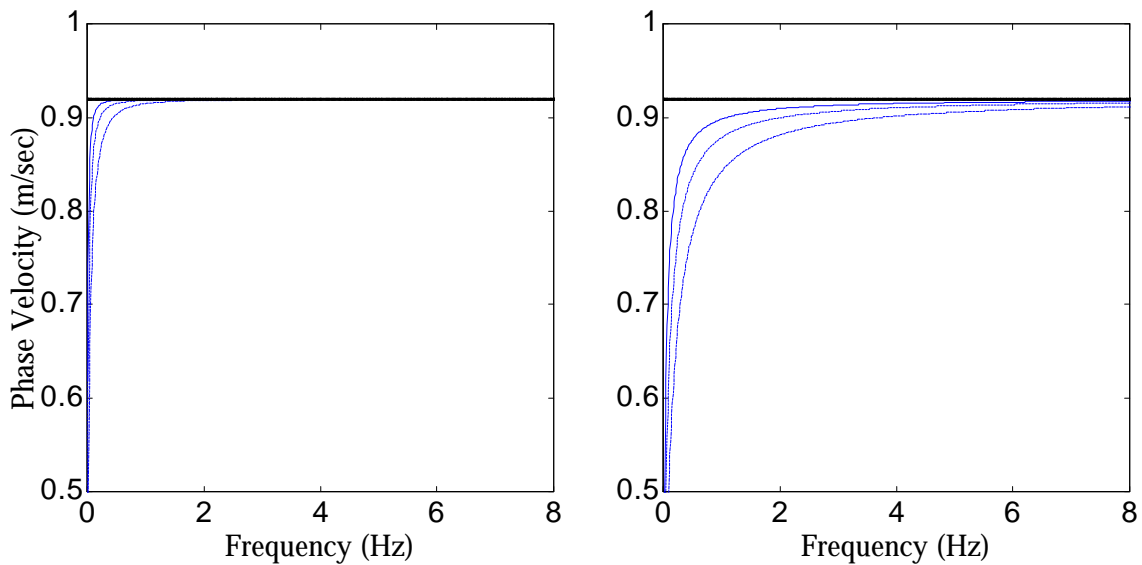


Figure 6.38 Sequence of Dispersion Curve Estimates for Traditional Cross Power (left panel) and Transfer Function (right panel) Method Estimators in a Homogeneous Half-Space with  $V_R = 0.92$  as Distance from Source Increases. A dimensionless space has been used to emphasize comparisons with previous geotechnical numerical studies, i.e. Sanchez-Salinero (1987), and the wavelength at 0.92 Hz equals 1. The dispersion curves for a measurement distance from the source equal to 0.75 (dashed-dot line), 1.5 (dashed line), and 3.0 (solid line) are shown. The correct  $V_R = 0.92$  (dark solid line) is shown for reference. Notice the larger bias and slower convergence of the traditional two-point transfer function estimator.

Table 6.2 Traditional Near-Field Mitigation and Filtering Recommendations (Ganji et al., 1998)

	First Receiver	Receiver Spacing
Lysmer	$2.5\lambda < d_1$	---
Heisey et al.	$d_1 = \Delta d$	$0.333 \lambda < \Delta d < 2\lambda$
Sanchez-Salinerio et al.	$d_1 = \Delta d$	$2\lambda < \Delta d$
Roesset et al.	$0.5 \lambda < \Delta d < 2\lambda$	$0.5 d_1 < \Delta d < d_1$
Gucunski and Woods	---	$0.5 \lambda < \Delta d < 4\lambda$
Tokimatsu et al.	$0.25 \lambda < d_1 + \Delta d/2$	$0.0625 \lambda < \Delta d < \lambda$

None of the criterion are the same, and based on the error found due to the cylindrical wavefield, some of the methods will yield smaller phase velocity estimates in normally dispersive media because they allow the first receiver position to be closer to the source. The conflicting and arbitrary recommendations in Table 6.2 are due to the poor estimation capabilities of the traditional two-point estimators and the model incompatibility. The lower bound on the first receiver corresponds to the acceptable error from estimating a plane wavenumber in a cylindrical wavefield. In one recommendation, the lack of a lower bound indicates that the model incompatibility is not uniformly recognized in active seismic surface wave testing. The upper bound on the second receiver stems from limited energy availability from the source and spatial aliasing. Recall that spatial aliasing mitigation for the traditional estimators relies on unwrapping the phase from a low frequency, so the spacing of the sensors must be less than one-half the largest wavelength measured. The lack of an upper bound on the second receiver spacing in one recommendation indicates that aliasing criteria in spatial wavefields is not uniformly recognized in the geotechnical engineering literature.

#### 6.10.4.3 Constrained the Usefulness of Active Source Surface Wave Testing

The model incompatibility constrains the ability to estimate phase velocities at lower frequencies and larger wavelengths. In single mode wavefields, the traditional phase velocity estimators always underestimate the phase velocity at lower frequencies, and the transfer function method actually tends to a zero velocity as frequency tends to zero, regardless of the profile or material velocity. The impact on ability to retrieve usable experimental estimates is significant. In cases where a single mode dominates, the phase velocity can be estimated to much lower frequencies if the correct cylindrical physical model and array processing are used.

#### 6.10.4.4 Large Scatter of Traditional Estimators Decrease Test Acceptability

Possibly the most discouraging result of the model incompatibility is the loss of persuasive power concerning practicing geotechnical engineers. The large scatter of two-point phase velocity estimates used to determine an average, or apparent, dispersion curve and the apparent ad hoc and qualitative nature of the filtering requirements, evidenced by

the array of recommendations in Table 6.2, reduce the ability to attract practicing engineers to implement the surface wave tests in practice. The advanced conventional and adaptive array based methods, although conceptually more difficult, remove the qualitative nature of seismic surface wave testing.

### 6.11 Cylindrical Wavefield Beamformers

An error in the traditional two-point phase velocity estimator, especially for low frequencies, is introduced due to using the incorrect model for the wavefield. In addition, due to the difference in phase change, the cylindrical wavefield has unequally spaced zeros which follow a Bessel function solution. This section derives optimum cylindrical beamforming methods, which use a different set of constraints and a different steering vector. The following sections will show the following:

- 1.) The ability of array-based plane wave estimators to handle the model

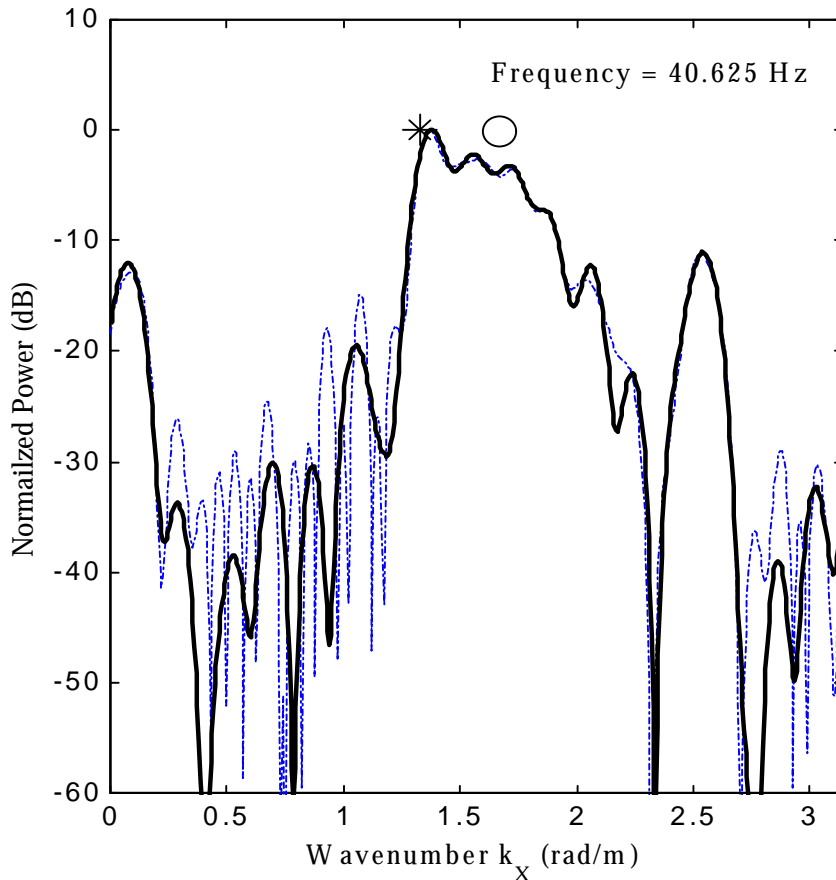


Figure 6.39 Power Spectrum Estimate for FDBF (dashed line) and Cylindrical HFDBF (heavy solid line) Methods Utilizing All 15 Sensors. Traditional estimators are shown with the asterisk and circle.

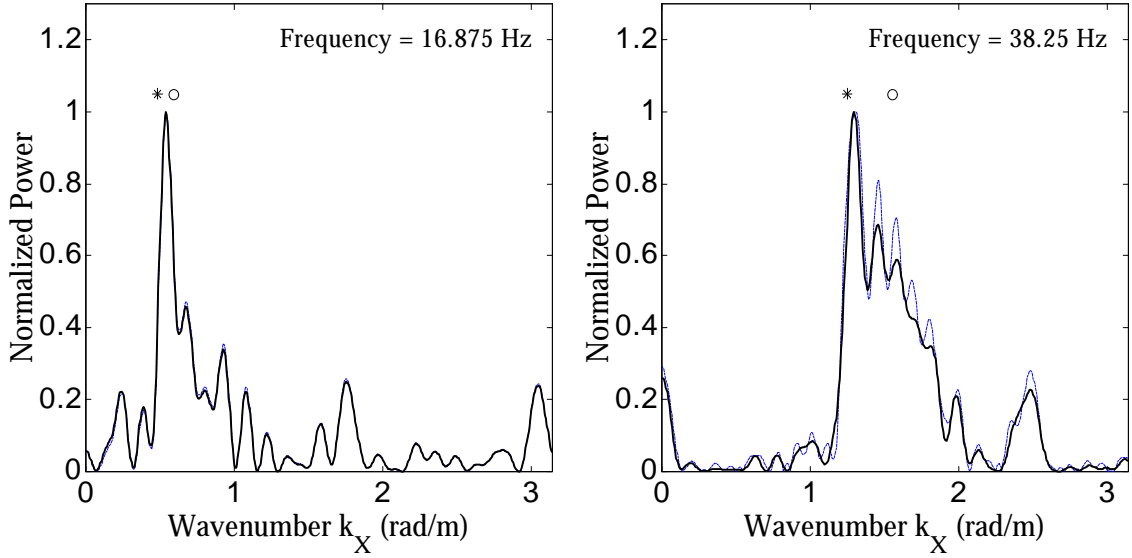


Figure 6.40 Cylindrical HFDBF (solid line) and FDBF (dashed line) Power Spectrum Estimates Using All 15 Sensors

- incompatibility if the array length is long enough,
- 2.) The ability of the cylindrical beamformers to estimate phase velocities for relatively long wavelengths compared to the array length.

#### 6.11.1 Cylindrical Frequency Domain Beamformer

The FDBF essentially takes the spatial Fourier transform of the spatio-spectral correlation matrix along the columns and then along the rows to estimate the frequency-wavenumber power spectrum. The Fourier transform uses plane wave, complex exponentials to line up the energy propagating past the array of sensors. The derivation of a cylindrical beamformer simply uses the Hankel transform rather than the Fourier transform.

Define the cylindrical steering vector as

$$\mathbf{h}(\mathbf{k}) = \exp\{-j[\phi(H_0(\mathbf{k} \cdot \mathbf{x}_1)) \quad \phi(H_0(\mathbf{k} \cdot \mathbf{x}_2)) \quad \cdots \quad \phi(H_0(\mathbf{k} \cdot \mathbf{x}_S))]\}^T \quad (6.12)$$

where  $\phi$  denotes taking the phase angle of the argument in parentheses. Equation 6.12 shows the unity magnitude of the cylindrical steering vector, and the Hankel function  $H_0$  allows the sensors to be aligned with the Bessel function phase rather than the equally spaced complex exponential phase, as in the FDBF. Since the phase of the Hankel function is used, the cylindrical beamformer will also be called the Hankel Frequency Domain Beamformer (HFDBF) to avoid any confusion with the conventional FDBF. The cylindrical HFDBF power spectrum estimate equals

$$P_{\text{HFDBF}}(\mathbf{k}, \omega) = \mathbf{h}^H(\mathbf{k}) \mathbf{R}(\omega) \mathbf{h}(\mathbf{k}) \quad (6.13)$$

The FDBF and HFDBF wavenumber power spectrum estimates at frequency = 40.625 Hz are shown in Figure 6.39. Two additional power spectrums are shown in Figure 6.40, and the peaks are very similar. The array smoothing function differs between the FDBF and HFDBF, due to a difference in the orthogonality properties of the transform kernels, i.e. the orthogonality of complex exponentials and Hankel functions are different. Figure 6.41 shows the array smoothing function for the ISC '98 synthetic linear array for the FDBF and HFDBF. The HFDBF has a narrower mainlobe width and larger sidelobes than the FDBF.

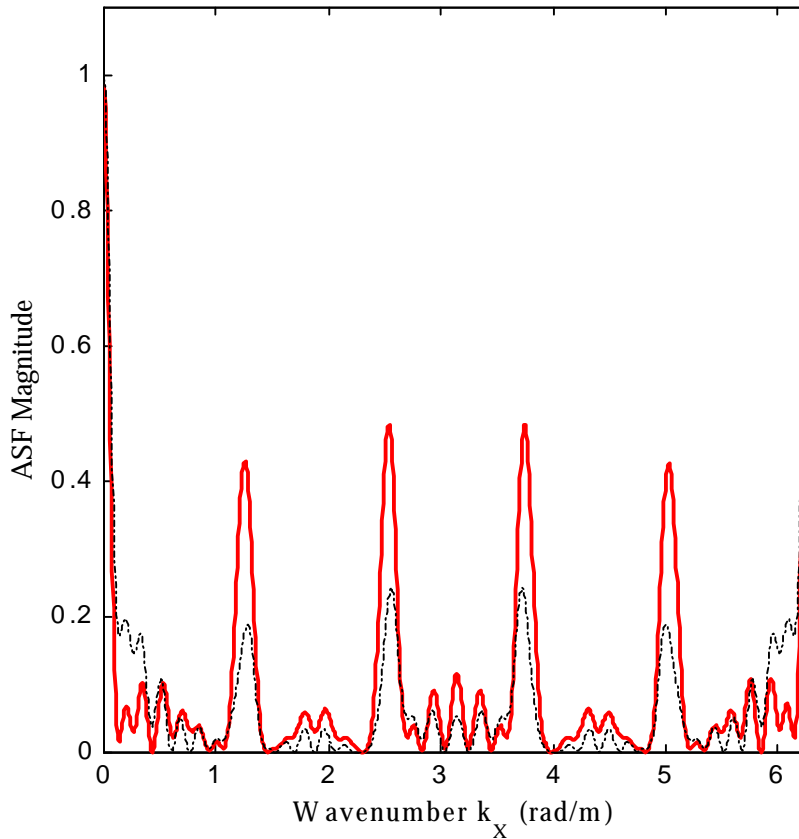


Figure 6.41 Array Smoothing Functions for the Cylindrical HFDBF (solid line) and FDBF (dashed line) for the ISC '98 Synthetic Linear Array. The Cylindrical HFDBF shows increased resolution and larger sidelobes than the FDBF.

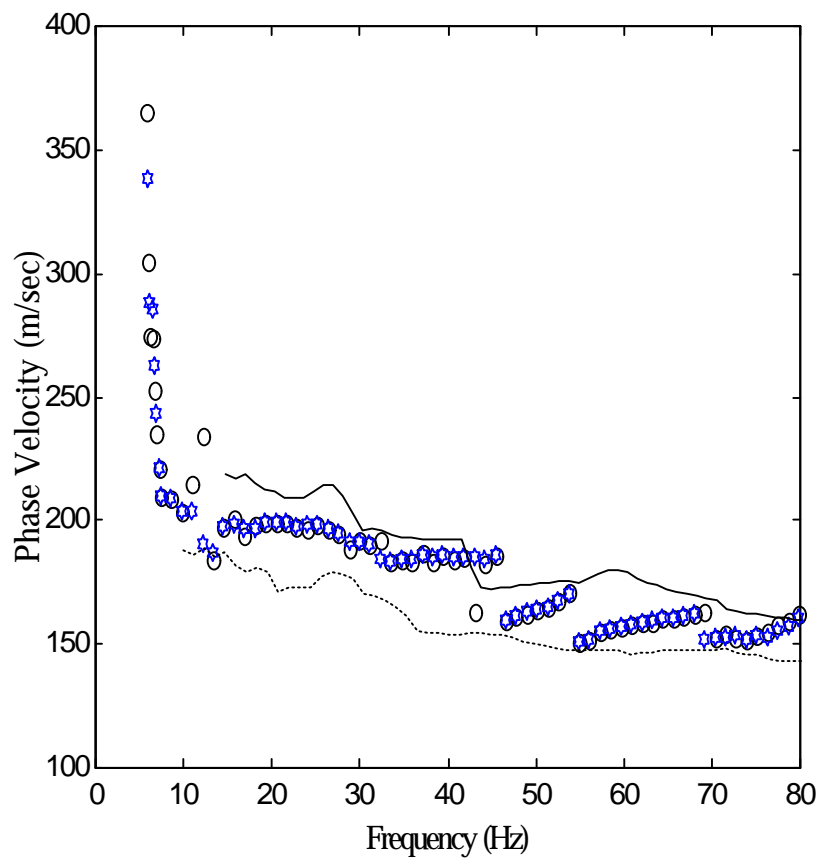


Figure 6.42 Cylindrical HFDBF Dispersion Curve Estimate. The cylindrical HFDBF estimate using all 15 sensors in the ISC '98 synthetic linear array is shown with stars, and the FDBF (circles) and traditional estimates (solid and dashed line) are shown for reference.

Figure 6.42 shows the HFDBF dispersion curve estimate for the ISC '98 site using all 15 sensor lags. The HFDBF and FDBF estimates appear to be almost identical, displaying the increased abilities of the advanced plane wave spectrum estimators to handle the near-field model incompatibility. Figure 6.43 shows a plan view of the HFDBF frequency-wavenumber power spectrum estimate. Figure 6.44 shows the percent difference between the FDBF and HFDBF phase velocity estimates shown in Figure 6.42. The percent difference equals zero for most frequencies, and is less than 10 percent in most cases.

To emphasize the impact of the cylindrical wavefield closer to the source, Figure 6.45 shows the HFDBF and FDBF power spectrum estimates using only sensors 1 to 8, corresponding to a maximum lag of 10 m. The HFDBF estimates a larger velocity, especially at lower frequencies, and the two methods tend to converge to the same estimate at larger frequencies. At lower frequencies, the reduced estimate of the phase velocities compared with Figure 6.42 is due to a decrease in resolution when using an array length of 10 m. Also, the phase velocity estimates at lower frequencies in Figure 6.45 probably represent a mix of several modes due to the reduced resolution.

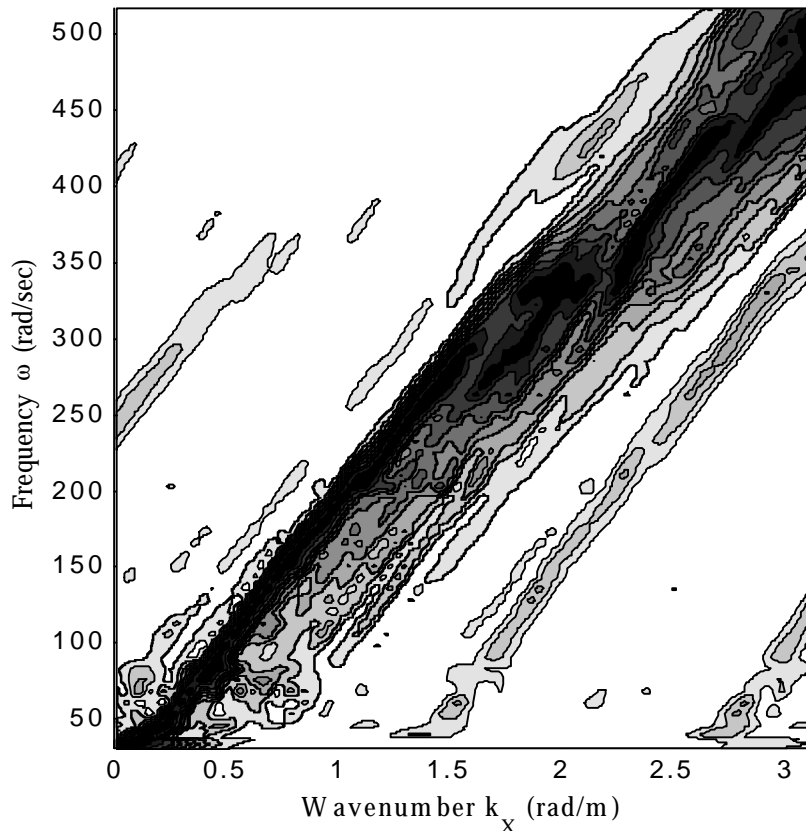


Figure 6.43 Cylindrical HFDBF Frequency-Wavenumber Power Spectrum Estimate

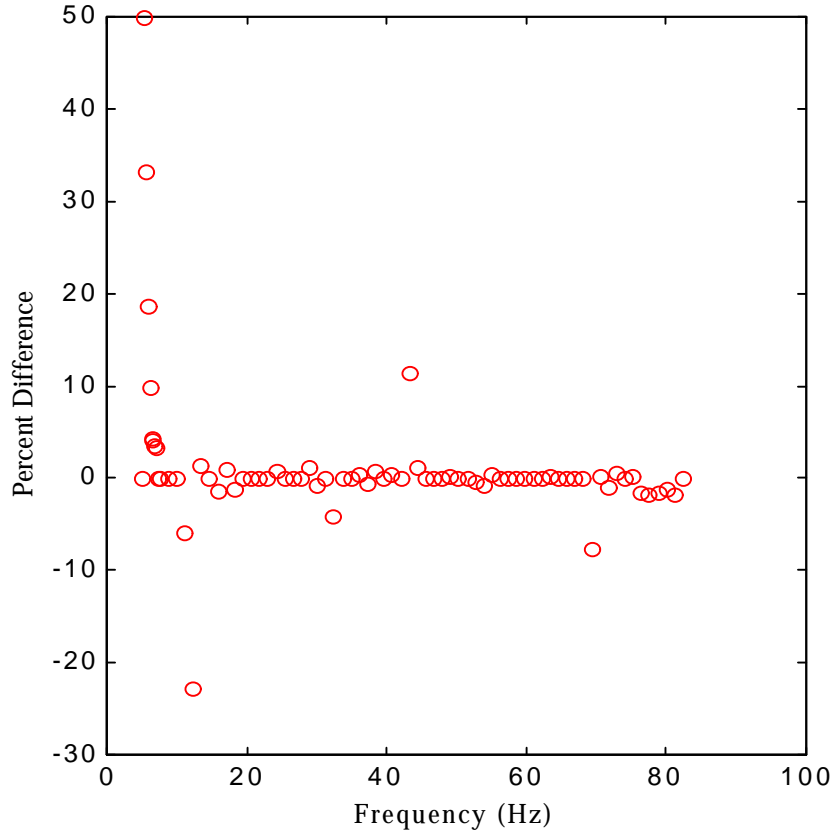


Figure 6.44 Percent Difference Between the Cylindrical HFDBF and FDBF Phase Velocity Estimates Using All 15 Sensors

Figure 6.46 (left panel) emphasizes the change in the peak location between the FDBF and HFDBF estimators at a frequency = 10.93 Hz. The peak wavenumber location of the HFDBF is slightly to the left of the FDBF peak, and therefore, the HFDBF estimates a larger phase velocity. The right panel of Figure 6.46 shows the percent difference between the FDBF and HFDBF phase velocity estimates using only the first eight sensors. The percent difference is almost a monotonically decreasing function of frequency. The 10 percent difference occurs at a frequency of about 6 Hz, corresponding to a wavelength of about 26 m. The one percent difference point occurs at about 20 Hz, corresponding to a wavelength of about 8 m. The difference converges to zero as frequency increases, showing the experimental estimates support the asymptotically unbiased nature of the plane wave estimators.

#### 6.11.2 Cylindrical Minimum Variance Distortionless Look

The MVDL is the solution to an explicit optimization problem, and therefore, derivation is more detailed than the FDBF estimator. The derivation of a cylindrical MVDL method, which will also be called the Hankel MVDL method (H MVDL), follows the same formulation as the MVDL derivation in Chapter 4. The constraints now become Hankel

function phase constraints, rather than complex exponential constraints, and the power estimate is

$$P_{\text{HMVDL}}(\mathbf{k}, \omega) = \frac{1}{\mathbf{h}^H(\mathbf{k})\mathbf{R}(\omega)^{-1}\mathbf{h}(\mathbf{k})} \quad (6.14)$$

where  $\mathbf{h}(\mathbf{k})$  is defined in Equation 6.12. The HMVDL attempts to pass with unity gain a cylindrical wave propagating with a given wavenumber, while optimally suppressing competing cylindrical waves and noise.

Figure 6.47 shows the 15 sensor synthetic linear array HMVDL and MVDL power spectrum estimates for two frequencies. Figure 6.48 shows the difference in the optimal weights calculated for the HMVDL and MVDL methods, and although the weights differ

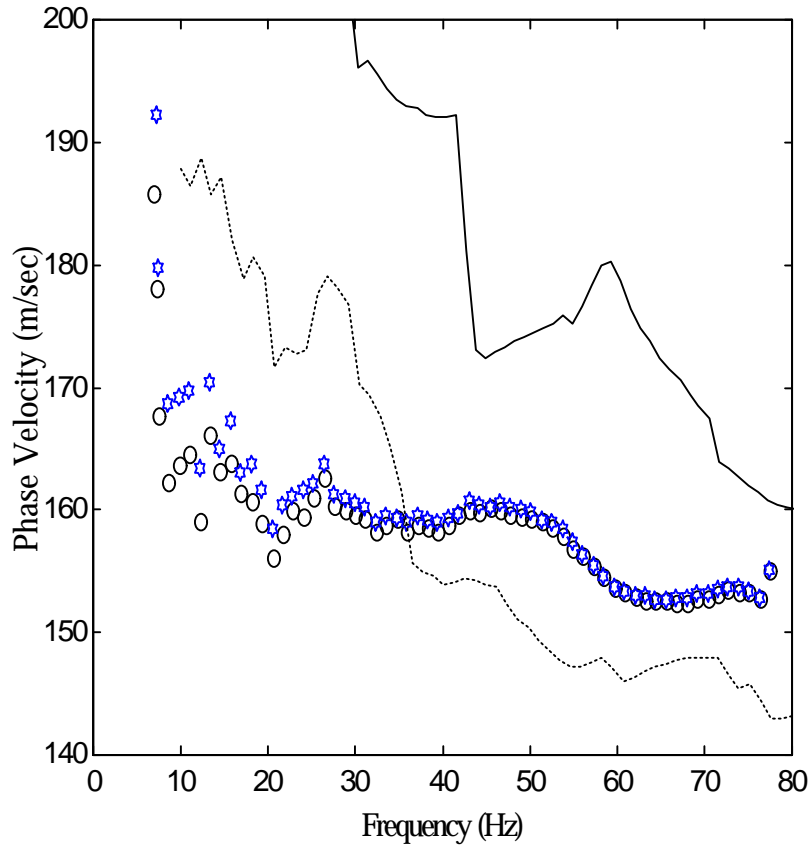


Figure 6.45 Dispersion Curve Estimate for the Cylindrical HFDBF (stars) and FDBF (circles) Methods Using Only Sensors 1 to 8. The total array length for sensors 1 to 8 is 10 m. The cylindrical HFDBF estimates larger phase velocities at all frequencies due to mitigating near-field model incompatibility effects.

considerably, the spectrum estimates are very similar. The HMVDL and MVDL dispersion curves using all 15 sensors in the ISC '98 synthetic linear array are shown in Figure 6.49. The phase velocity estimates are very similar, and Figure 6.50 shows that the percent difference between the HMVDL and MVDL phase velocity estimates is zero for almost all frequencies. Figure 6.51 shows a plan view of the HMVDL frequency-wavenumber spectrum.

Figures 6.52 and 6.53 analyze the difference in MVDL and HMVDL phase velocity estimates for sensors 1 to 8. Similar to the FDBF analysis, the HMVDL estimates higher velocities at lower frequencies, and the two methods converge as frequency increases.

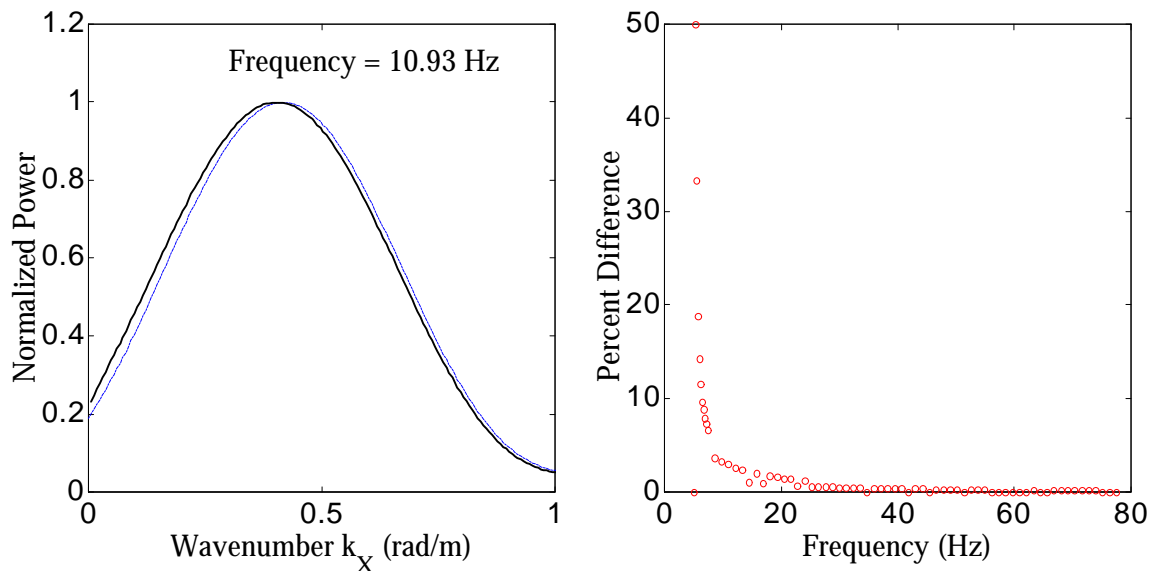


Figure 6.46 Cylindrical HFDBF Versus FDBF Estimates Using Only Sensors 1 to 8. Close up of peak location of Cylindrical HFDBF (solid line) and FDBF (dashed line) power spectrum estimates at a frequency = 10.93 Hz are shown in the left panel, and the percent difference between the Cylindrical HFDBF and FDBF phase velocity estimates when using only sensors 1 to 8 are shown in the right panel. Notice the monotonically decreasing estimation difference as frequency increases.

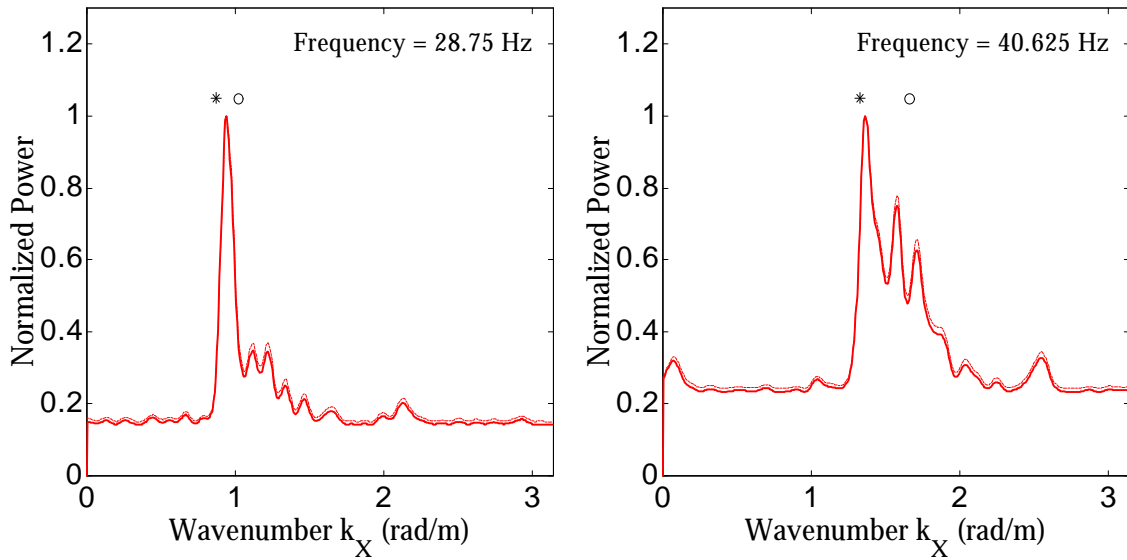


Figure 6.47 Cylindrical HMVDL and MVDL Power Spectrum Estimates for 15 Sensor ISC '98 Linear Array

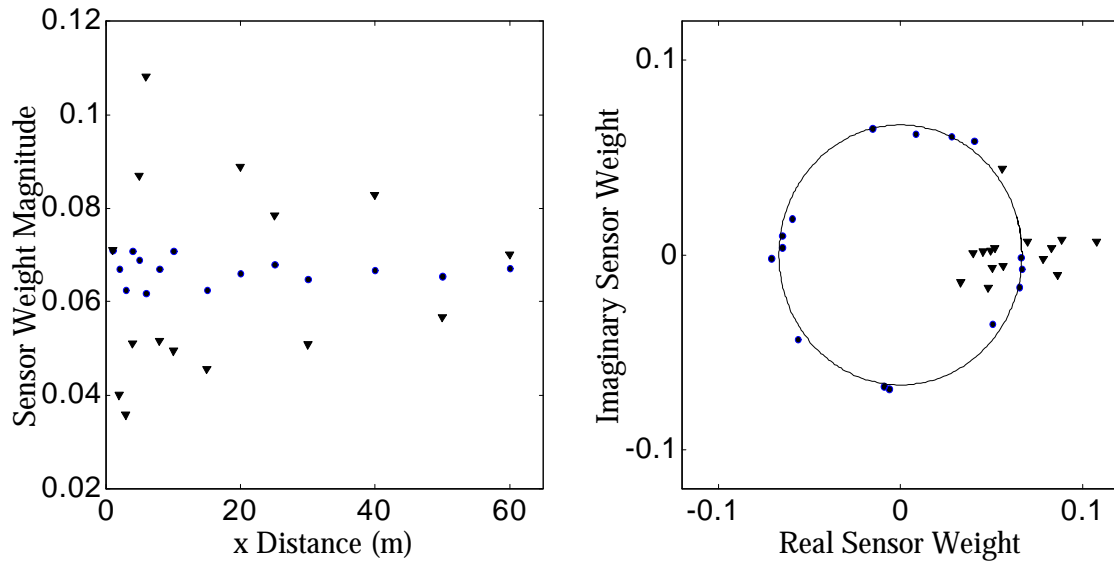


Figure 6.48 Magnitude and Complex-Valued Weights for the Cylindrical HMVDL and MVDL Methods. The magnitude (left panel) and complex-valued (right panel) weights are shown for the cylindrical HMVDL (triangles) and MVDL (circles) methods at a frequency = 28.75 Hz and a dominant wavenumber = 0.945 rad/m.

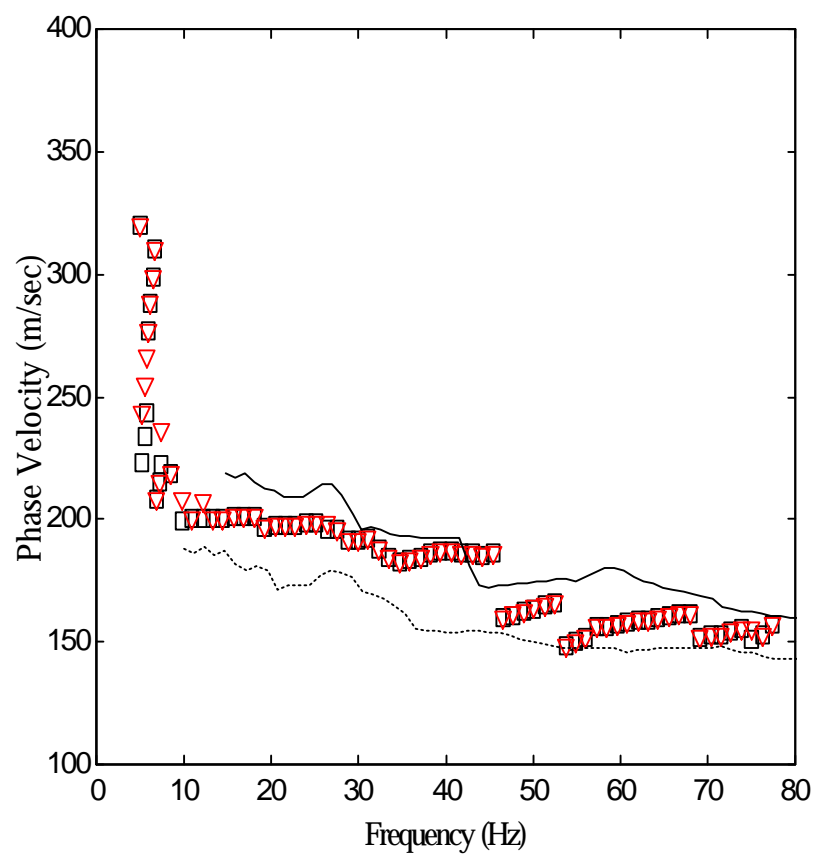


Figure 6.49 Dispersion Curve Estimates for Cylindrical HMVDL (triangles) and MVDL (squares) Methods Utilizing All 15 Sensors in ISC '98 Linear Array

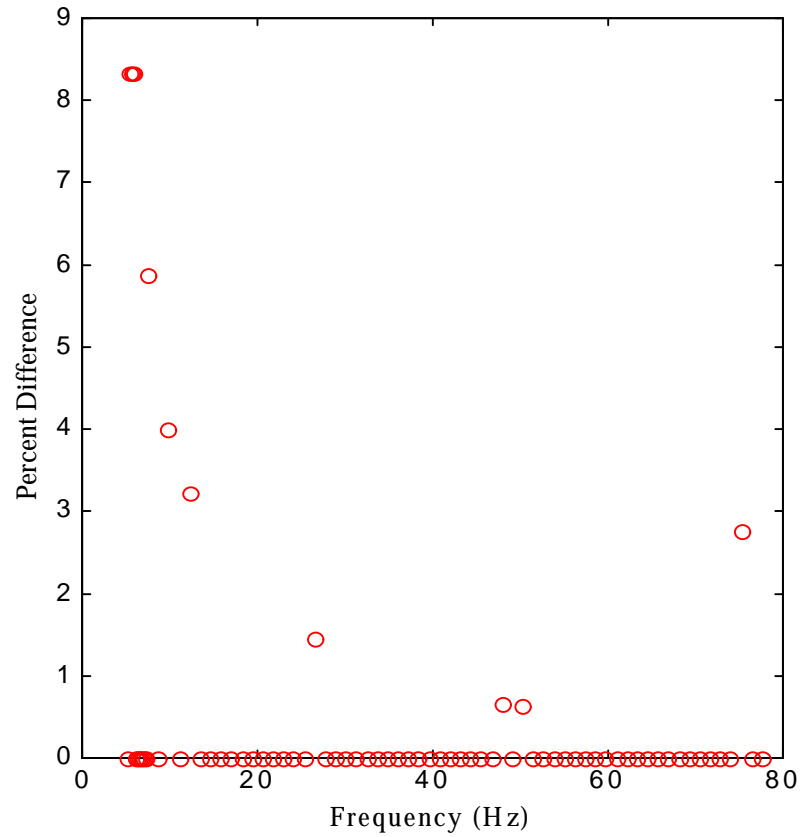


Figure 6.50 Percent Difference Between Cylindrical HMVDL and MVDL Phase Velocity Estimates Using All 15 Sensors. Compared to the FDBF (see Figure 6.44), the MVDL yields a significantly smaller error due to the near-field modeling incompatibility.

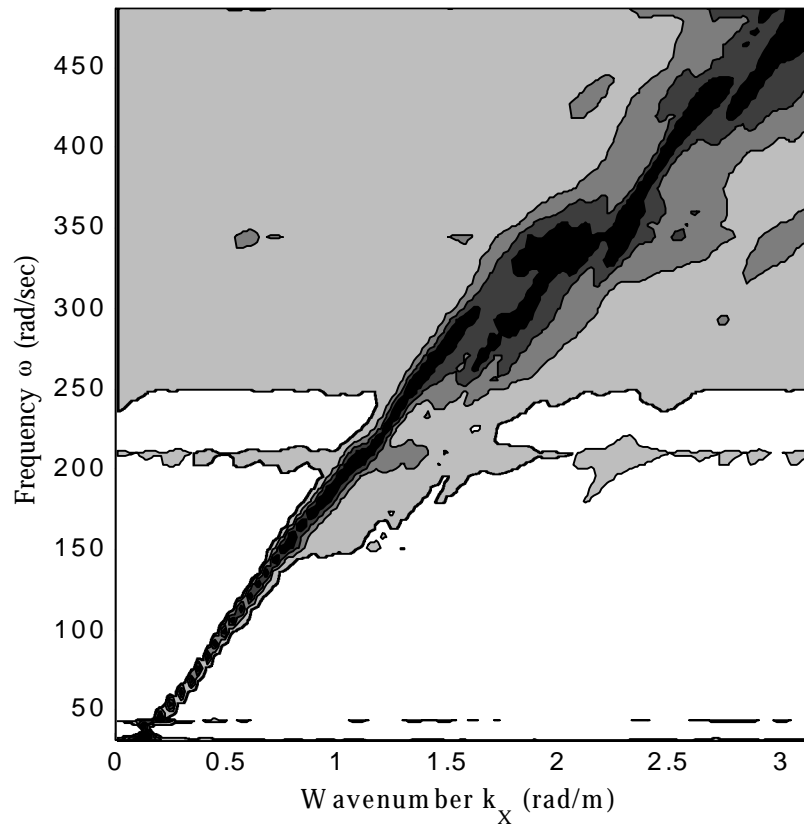


Figure 6.51 Cylindrical HMVDL Frequency-Wavenumber Power Spectrum Estimate Utilizing All 15 Sensors in the ISC '98 Synthetic Linear Array

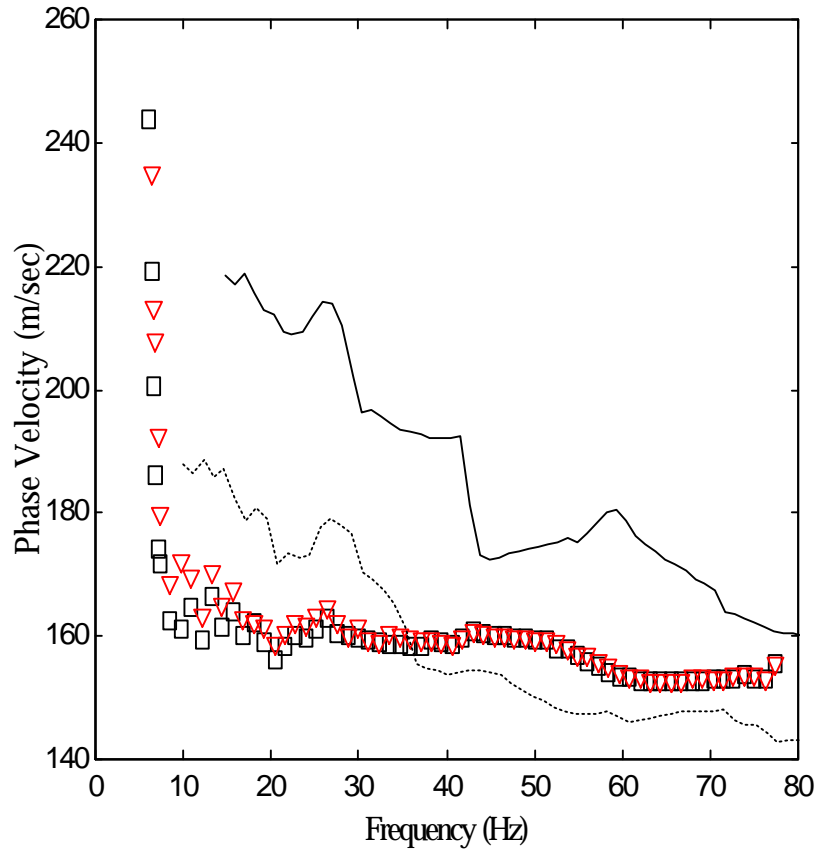


Figure 6.52 Dispersion Curve Estimate for the Cylindrical HMVDL (triangles) and MVDL (squares) Methods Using Only Sensors 1 to 8. The total array length for sensors 1 to 8 is 10 m. The cylindrical HMVDL estimates larger phase velocities at all frequencies due to the mitigation of near-field model incompatibility effects.

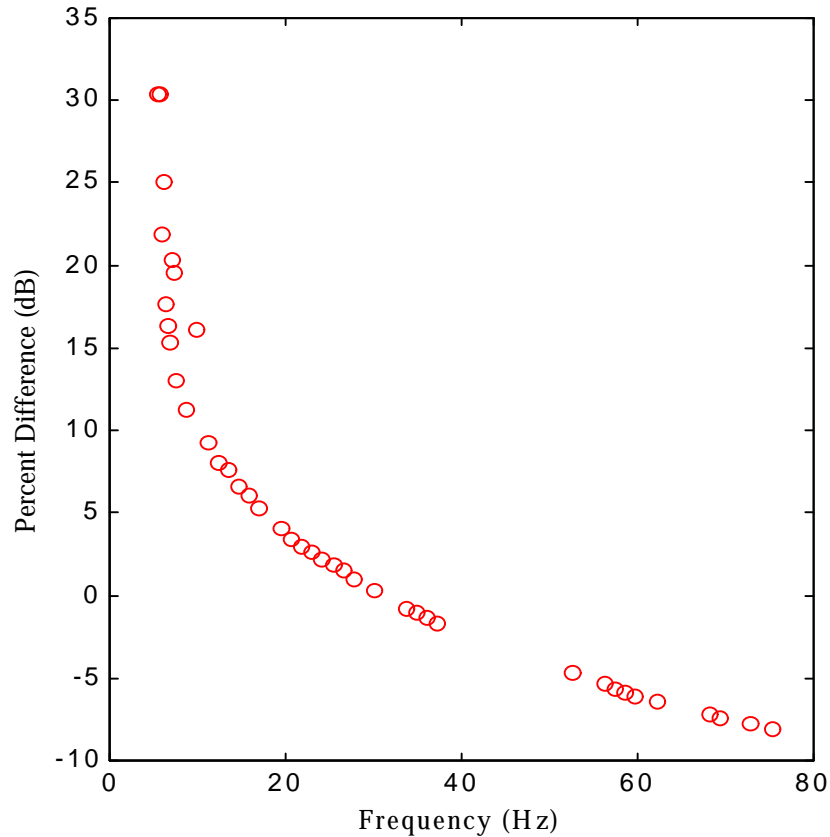


Figure 6.53 Percent Difference Between Cylindrical HMVDL and MVDL Phase Velocity Estimates Using Only Sensors 1 to 8. Zero dB corresponds to a 1 percent difference in the estimates.

### 6.12 Plane Wave Versus Cylindrical Wave Beamformers

Using the correct physical model offers better phase velocity estimates but requires greater numerical calculation. The plane wave estimators allow efficient use of the FFT, as discussed in Appendix A; on the other hand, cylindrical beamformer steering vectors must be calculated numerically for each possible wavenumber. Compared to the traditional two-point phase velocity estimators, the conventional and adaptive plane wave estimation methods control the near-field error to a great extent, due to the integration of information over a larger spatial range. Considering the percent difference of the results between the cylindrical and plane wave array-based estimation methods presented in this section, the plane wave array estimators yield excellent estimates except at low frequencies or for short array lengths. Due to the increased calculating speed and ease of interpretation, the plane wave estimators will be used for the remainder of this chapter, unless otherwise noted.

### 6.13 Multiple Mode Estimation

Extraction of multiple modes offers significant gains in information and the ability to determine a more unique inverted soil profile. Although peak picking in the wavenumber spectrum offers the simplest method to retrieve multiple modes, several disadvantages,

especially when using only 15 sensors lags, exist in the simple peak picking method. First, the presence of multiple propagating signals result in biased peak estimates, typically with the bias increasing as the signals become closer together. Second, the possibility of misclassification of a sidelobe as a signal exists when dealing with imperfect spectral smoothing kernels. Third, sidelobes due to large amplitude signals can mask the identification of smaller amplitude signals. Fourth, the superposition of several signals results in sidelobes of each signal contributing to more remote portions of the spectrum. Depending on the location of sidelobes and signals, the ordering of the modes with respect to energy content may be improperly determined if the engineer solely relies on peak picking methods. Although the adaptive methods reduce the magnitude of the previously mentioned problems, as long as a limited number of sensors are deployed, the problems will be manifested in peak picking methods.

Since the ISC '98 synthetic linear array includes only 15 sensors, and in many cases, practicing engineers will deal with limited experimental measurements, a more robust method of determining multiple mode wavenumbers and modal power ratios is necessary. Assuming the largest peak in the power spectrum estimate is due to a propagating signal, the smoothing kernel associated with that signal is removed and the next highest peak is chosen as the second mode of propagation (Nolet, 1976; Aki and Richards, 1980). Nolet (1976) subtracted the MVDL smoothing kernel, which depends on both the frequency and wavenumber, and therefore, changes form for each frequency and mode being estimated. Although the method can be used with any spectrum estimator in which an array smoothing function has meaning, a method using only the FDBF method is presented. The FDBF is used for the following reasons:

- 1.) The FDBF offers the most efficient implementation, if concern over speed of calculation is an issue, because of the ease of utilizing the FFT with linear arrays, and non-necessity of calculating matrix inverses,
- 2.) The FDBF method is easiest to understand and implement because the array smoothing function exhibits a constant structure. The FDBF is a linear method, in the terminology encountered in advanced signal processing, because the filter structure is identical regardless of which spectral component is being estimated. In comparison, the MVDL is considered a non-linear method because the scaling of a single spectral component estimate depends on the mainlobe width and sidelobe structure of the filter (Haykin, 1979).

In the desire to motivate the use of multiple mode extraction, the FDBF offers the most tractable implementation method, allows an easy progression to the use of more advanced multiple mode extraction methods, and, as seen in the following sections, will offer excellent results in many cases.

Figure 6.54 shows the power spectrum estimate after removing the dominant mode for a frequency = 28.75 Hz. Removal of the dominant mode smoothing function allows the second mode to be seen more clearly. Since the dominant mode normalized power is considered equal to one, and the actual amplitude estimate is due to the dominant signal plus sidelobes of other signals and noise, the power estimate after removing the dominant mode may be less than zero at some frequencies. More advanced and iterative methods could be used to minimize the effects of misestimating the dominant signal amplitude. To help ensure a second mode is being estimated, only power ratios, relative to the first mode, greater than 0.4 were used. The cutoff is rather arbitrary, but the extraction of multiple modes from only 15 sensors should not be used without restraint.

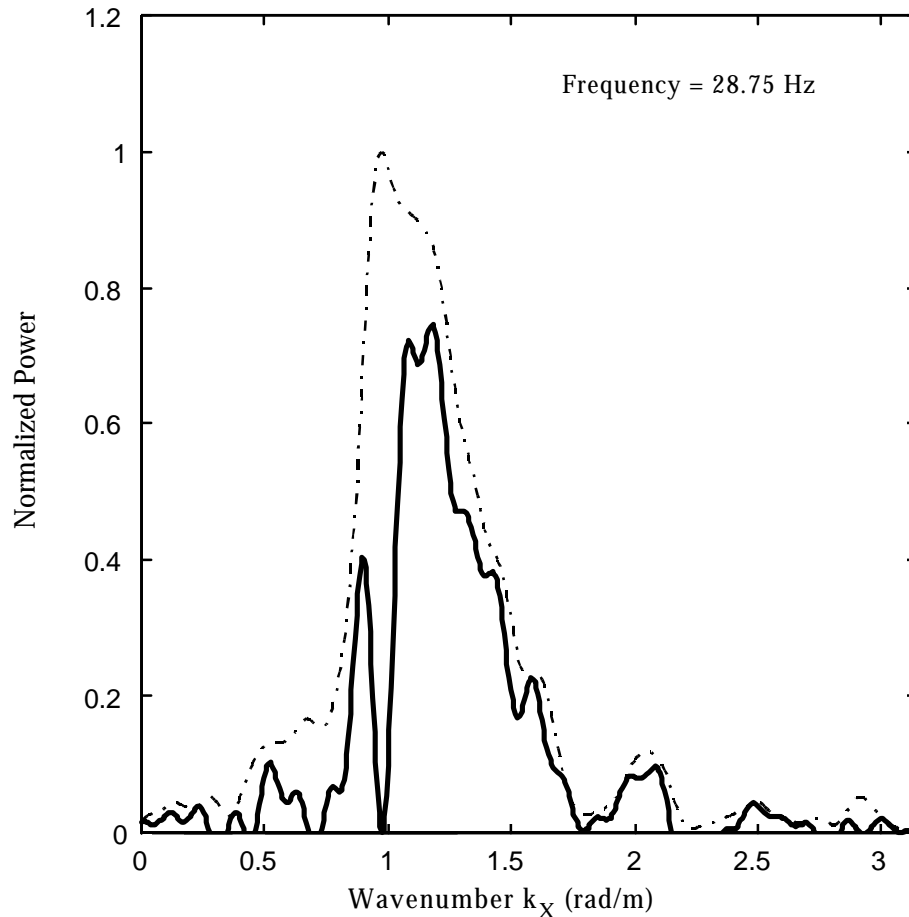


Figure 6.54 Extraction of Mode with Second Highest Energy Content

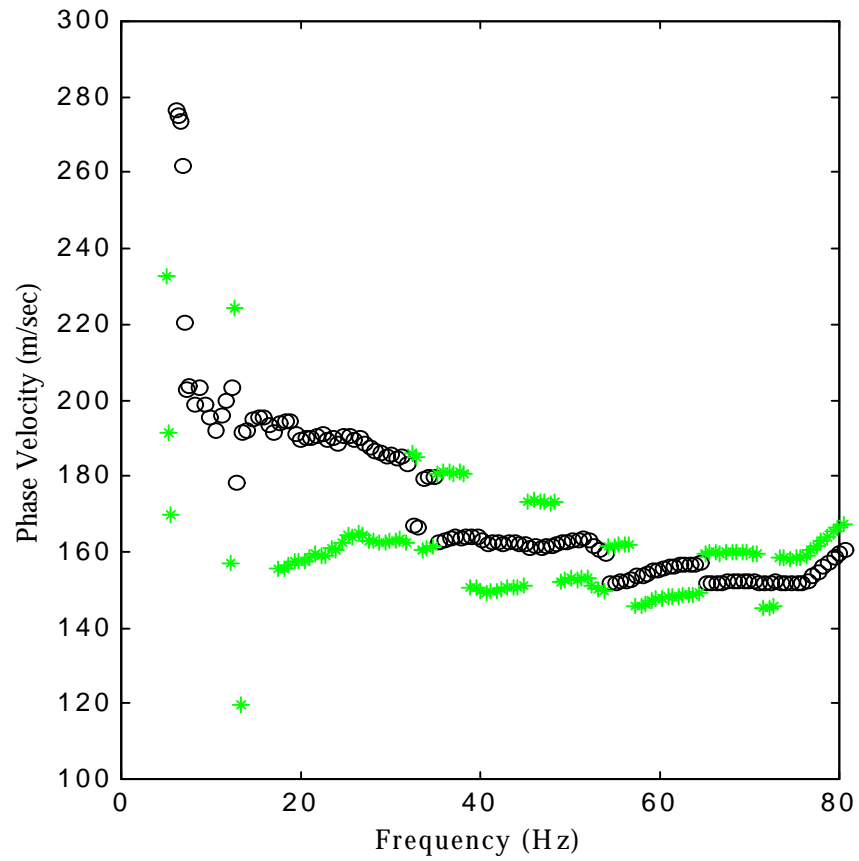


Figure 6.55 Multiple Mode Dispersion Curve. Multiple mode dispersion curve displaying the phase velocity estimates from the wavenumbers with the two greatest energy contents at each frequency. The circles contain greater energy than the asterisks.

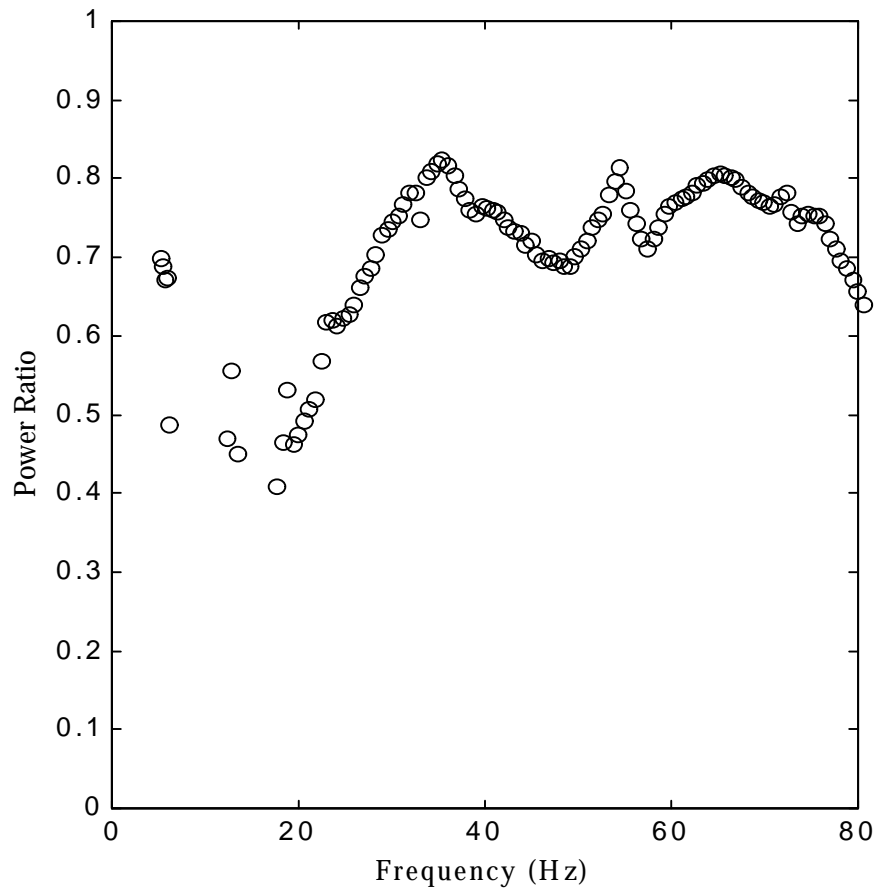


Figure 6.56 Power Ratios of Multiple Modes. The power ratios of the two modes shown in Figure 6.55, expressed as the second highest energy mode divided by the dominant energy mode.

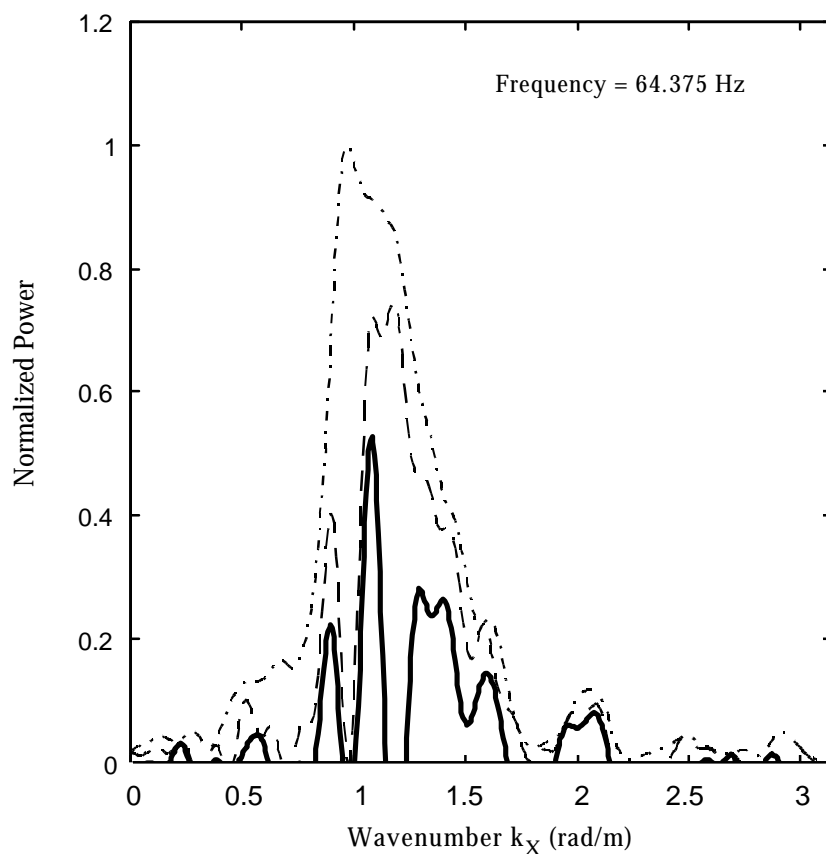


Figure 6.57 Estimation of Wavenumber with Third Greatest Energy Content. Power spectrum estimate (dark solid line) at a frequency = 64.375 Hz after the removal of the two highest energy modes. The original power spectrum (dash-dot line) and the power spectrum after removing the dominant mode (dashed line) are shown for reference.

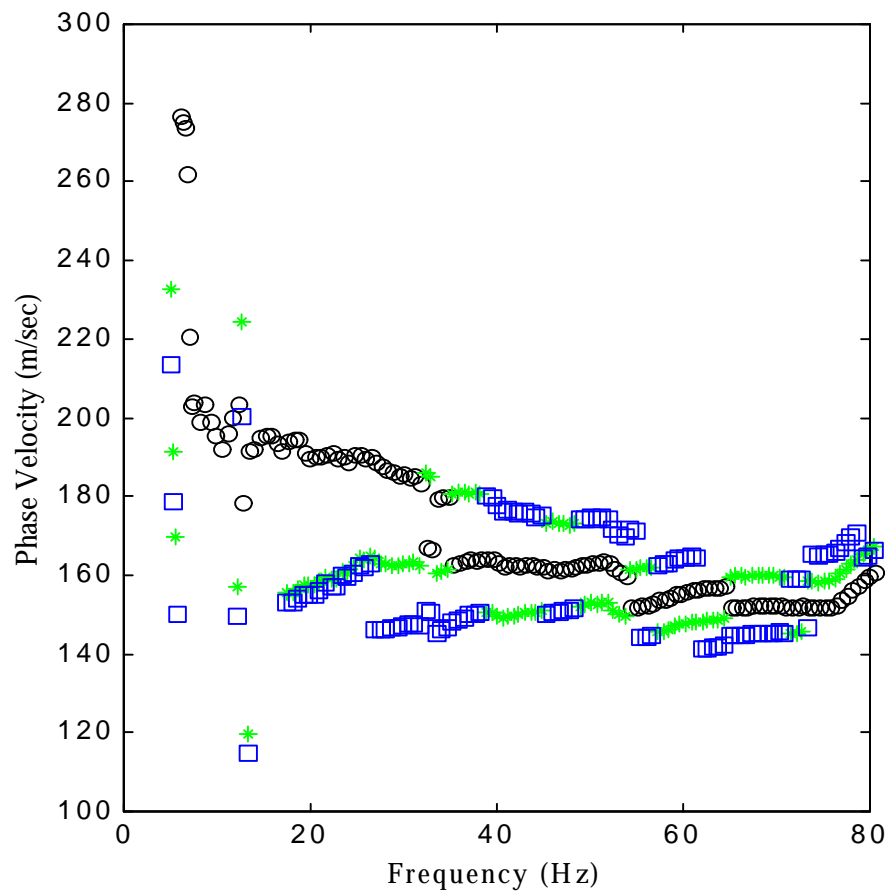


Figure 6.58 Dispersion Curve Estimate Including the Mode with the Third Greatest Energy Content. The modes containing the third greatest energy (squares), the second greatest energy (asterisks), and the greatest energy (circles) are shown.

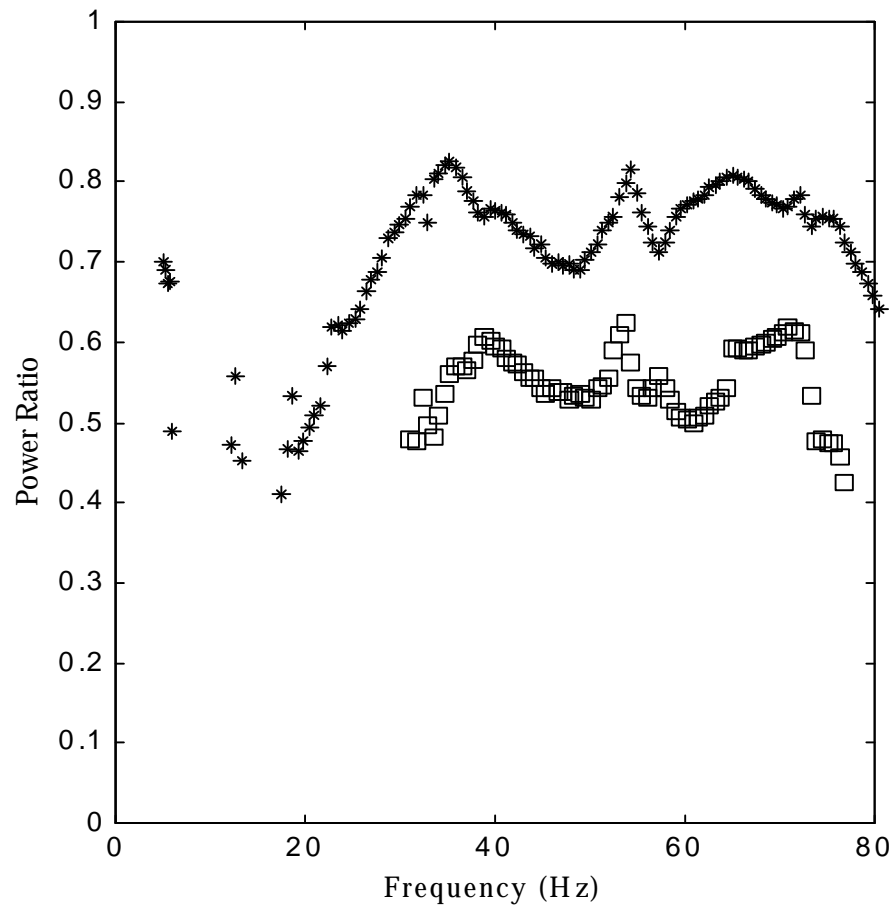


Figure 6.59 Multiple Mode Power Ratios. The power ratio of second (asterisks) and third (squares) highest energy modes relative to the dominant energy mode are shown. Notice the apparent resonance near 40, 55 and 70 Hz.

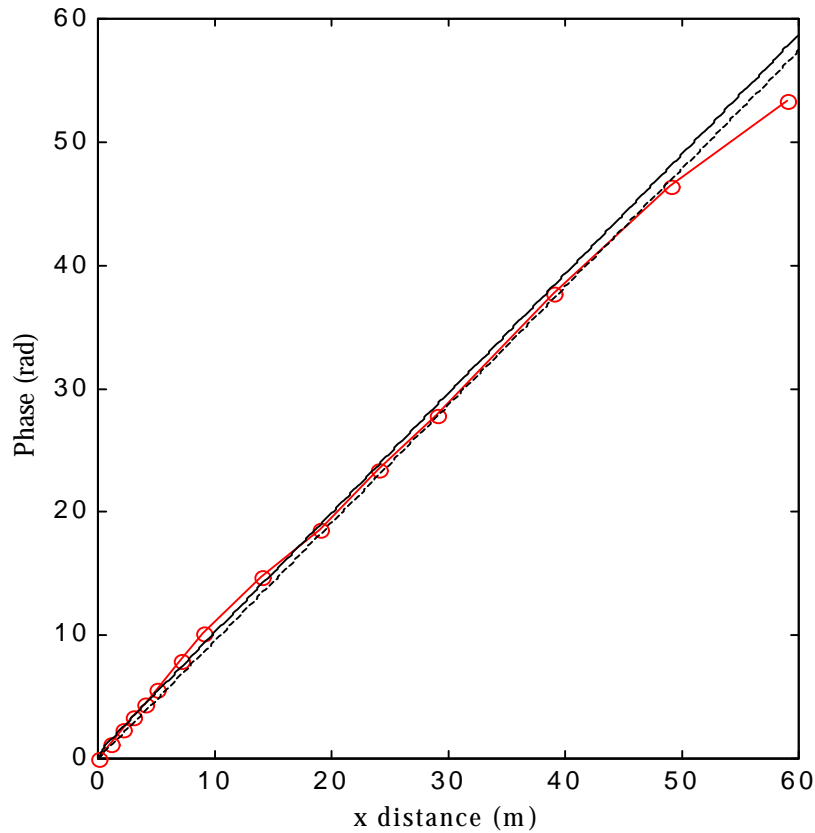


Figure 6.60 Phase Versus Lag Distance for the ISC '98 Site at a Frequency = 28.75 Hz. Experimental measurements (circles), dominant mode FDBF estimate (dashed line), and dominant mode Cylindrical HFDBF estimate (solid line) are shown.

Figure 6.55 shows the dispersion curve estimate including the two modes with the greatest energy content. The second mode appears to fill in the gaps of the dominant mode. Figure 6.56 shows the power ratio of the mode with the second greatest energy content relative to the dominant mode. A resonance effect appears to occur near 40 and 55 Hz.

Figure 6.57 shows an example of the isolation of a third mode of propagation, and Figure 6.58 shows the dispersion curve estimated from the three modes with the greatest energy content. The third mode appears to continue the trends of the previous modes. Figure 6.59 shows the power ratio of the mode with the third greatest energy content.

Two features of the multiple mode power ratio graphs should be emphasized. First, the power ratios of the second and third greatest energy content modes show a resonance phenomenon at about 40, 55, and 70 Hz. The resonance phenomenon is not unexpected, since the multiple modes are due to reflections at material boundaries and the amount of energy reflected depends on the layering characteristics, angle of incidence, and material properties. Second, the fundamental mode does not dominant.

#### 6.14 Signal Modeling

A detailed analysis of phase versus spatial lag will clarify several of the important concepts relating to seismic surface wave modal superposition and phase velocity estimation, including the reasons underlying the relative positions of the traditional phase velocity estimators. Figures 6.60 and 6.61 show the experimental phase measurements and the fit of the dominant energy mode for a frequency = 28.75 Hz. The oscillatory character of the experimental measurements, due to the superposition of several modes, around the dominant mode is evident. The HFDBF estimate tends to fit the data better due to the ability to model the curved phase change near the source.

Figure 6.62 displays the physical reason the traditional two-point cross power spectrum method yields too low a wavenumber estimate, and therefore, too high a phase velocity estimate. Figure 6.63 shows a similar plot for the traditional transfer function method, which yields too high a wavenumber estimate and too low a phase velocity

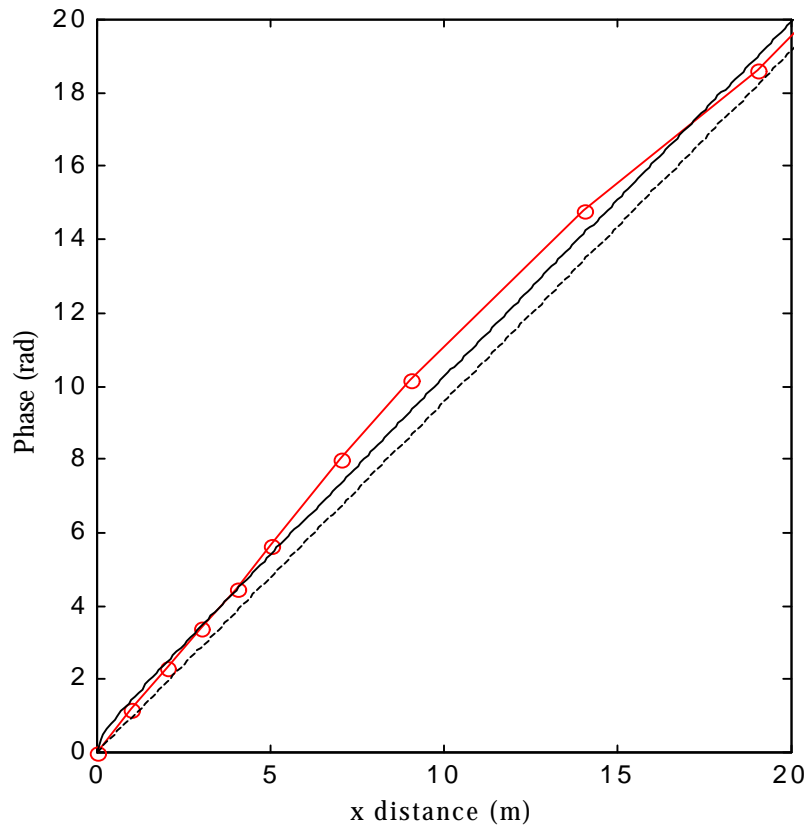


Figure 6.61 Close Up of Figure 6.60. The close-up emphasizes the apparent oscillation of the ISC '98 experimental phase measurements (circles) around the fundamental Cylindrical HFDBF (solid line) and FDBF (dashed line) estimates for a frequency = 28.75. The dominant energy mode wavenumber estimate for both the FDBF and the Cylindrical HFDBF equals 0.9695 rad/m.

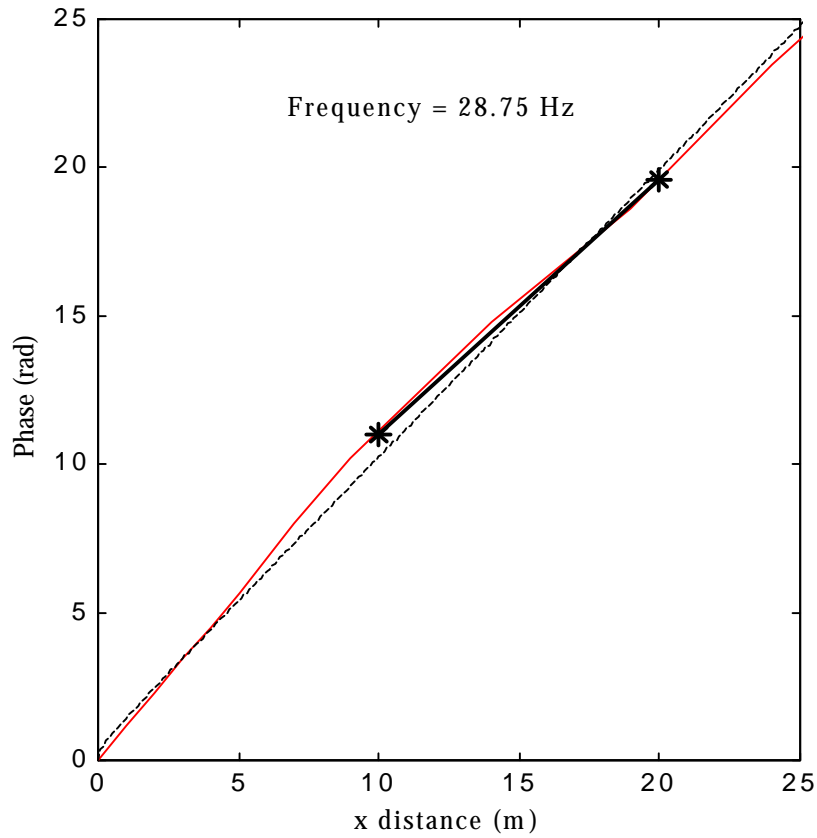


Figure 6.62 Traditional Two-Point Cross Power Estimate Model. The traditional two-point cross power spectrum estimation method (shown in asterisks and heavy line) yields too low a wavenumber estimate compared to the advanced estimator (shown in dashed line). The experimental measurements are shown for reference (solid line).

estimate for frequency = 28.75 Hz. Due to the superposition of several modes, the two-point method will estimate alternatively high and low phase velocity estimates depending on the choice of sensor locations, and example sensor locations are easily identifiable where the cross power spectrum will yield a lower phase velocity than the transfer function estimate.

Figures 6.62 and 6.63 are useful to discuss some of the common conclusions and recommendations relating to the traditional seismic surface wave estimators. First, the transfer function method has been noted to yield better estimates in experimental dispersion curves exhibiting resonance effects, since the transfer function method tends to smooth out some of the cross power method dispersion curve oscillations (Sanchez-Salintero, 1987). The transfer function method yields smoother results due to averaging over larger spatial lags.

Second, the recommendation of using a receiver 1 to receiver 2 distance equal to at least 2 times the source to receiver 1 spacing really is stating that to estimate the phase velocity in a multimodal wavefield with traditional estimators, a minimum amount of averaging of spatial distance is required before an apparent mode manifests itself. The

recommendation of as large a ratio of spacings as possible is also stating that as large an averaging as possible is recommend due to the poor estimator properties of the traditional methods. Third, even in the far-field, multiple mode wavefields can produce negative phase velocity estimates for close receiver spacings when using the cross power method.

Figure 6.64 shows the fit of the three greatest energy modes, weighted by their respective estimated amplitude ratio, with the experimental phase measurements for frequency = 28.75 Hz. The fit is excellent. Chapter 7 will introduce attenuation and the fit of experimental magnitude measurements.

### 6.15 Alternative Phase Velocity Estimation Method

The original derivation of the MVDL method used the noise covariance matrix (Capon, 1969), which includes only noise, rather than the spatio-spectral correlation matrix, which includes signal plus noise. When the noise background field can be measured prior to introducing the signal, such as prior to the arrival of an earthquake event, the optimum sensor weights can be determined from the noise field. The underlying motivation for this

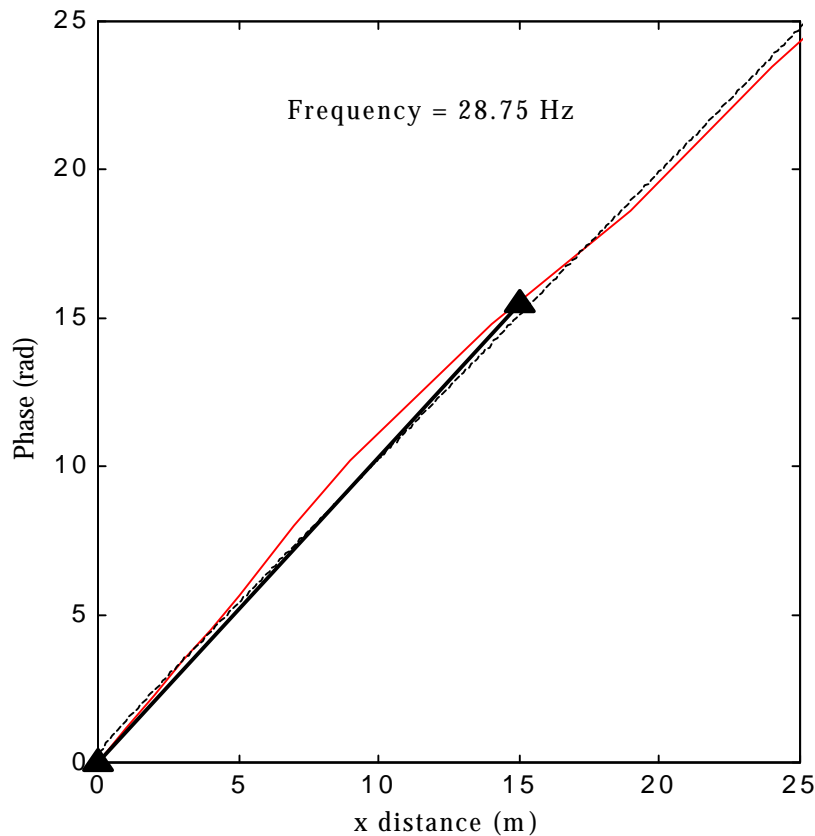


Figure 6.63 Traditional Two-Point Transfer Function Estimate Model. The traditional two-point transfer function method (shown in triangles and heavy line) yields too high a wavenumber estimate compared to the advanced estimator (shown in dashed line). The experimental ISC '98 measurements are shown for reference (solid line).

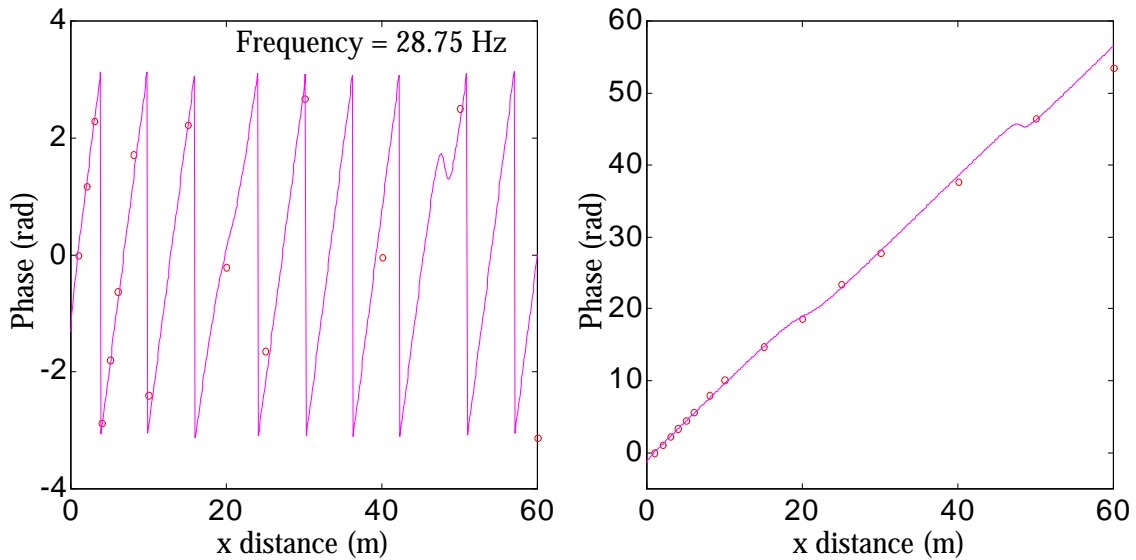


Figure 6.64 Multiple Mode Phase Change Model. The experimental ISC '98 phase measurements (shown with circles) and the fit of the three modes containing the greatest energy obtained with advanced power spectrum estimators (shown with solid line) for wrapped (left panel) and unwrapped (right panel) phase plots.

stems directly from the eigenanalysis concepts described in Chapter 4. The signal and noise are orthogonal components in the wavefield, and the optimum filter is designed simply by looking for components orthogonal to the noise. Since the active surface wave tests allow measurement of the ambient background wavefield before the introduction of the signal, the use of the noise covariance matrix is a simple extension. Note that problems such as stationarity of the background noise field remain very important.

#### 6.16 Summary and Conclusions

Spatial array processing allows considerable gains in information to be obtained from the traditional surface wave setup. Along with a few assumptions about the background noise wavefield, synthetic linear arrays can be derived. The advanced spectrum estimation techniques solve the common problems associated with traditional analysis of seismic surface waves. The three major problems identified in traditional seismic surface wave analysis are the following:

- 1.) The model incompatibility effect, which is due to using a plane wave estimator in cylindrical wavefields,
- 2.) Near-field body wave interference, due to reflecting body wave energy that does not contribute to additional Rayleigh surface wave modes,
- 3.) Far-field body wave interference, which is due to the inability of traditional estimators to account for multiple surface wave modes of propagation.

The conventional and adaptive plane wave synthetic array estimators yield considerable decreases in the effects due to the model incompatibility, and the introduction

of the correct Hankel function solution for cylindrical wavefields allows the development of optimum cylindrical beamformers. The Bessel function follows similar orthogonality properties as the complex exponential, and the smoothing function of the Hankel transform is similar to the complex exponential smoothing function encountered in Fourier analysis.

The resolution characteristics and effects of different normalization techniques were discussed. Although normalizing by the  $\sqrt{x}$  decay rate yields excellent results, the best normalization, as shown in Chapter 7, would use the correct wavenumber geometric attenuation rates. The model incompatibility effects were discussed in detail, due to their large impact on traditional geotechnical phase velocity estimators and recommendations. The common recommendations for near-field mitigation were shown to be dominated by the acceptable errors due to the model incompatibility. The advanced spectrum estimators have much better spatial filtering characteristics, and therefore, multiple modes and their power ratios can be extracted.